A general two-phase debris flow model

Shiva P. Pudasaini[1,2]

Received 10 August 2011; revised 25 May 2012; accepted 1 June 2012; published 1 August 2012.

[1] This paper presents a new, generalized two-phase debris flow model that includes many essential physical phenomena. The model employs the Mohr-Coulomb plasticity for the solid stress, and the fluid stress is modeled as a solid-volume-fraction-gradient-enhanced non-Newtonian viscous stress. The generalized interfacial momentum transfer includes viscous drag, buoyancy, and virtual mass. A new, generalized drag force is proposed that covers both solid-like and fluid-like contributions, and can be applied to drag ranging from linear to quadratic. Strong coupling between the solid- and the fluid-momentum transfer leads to simultaneous deformation, mixing, and separation of the phases. Inclusion of the non-Newtonian viscous stresses is important in several aspects. The evolution, advection, and diffusion of the solid-volume fraction plays an important role. The model, which includes three innovative, fundamentally new, and dominant physical aspects (enhanced viscous stress, virtual mass, generalized drag) constitutes the most generalized two-phase flow model to date, and can reproduce results from most previous simple models that consider single- and two-phase avalanches and debris flows as special cases. Numerical results indicate that the model can adequately describe the complex dynamics of subaerial two-phase debris flows, particle-laden and dispersive flows, sediment transport, and submarine debris flows and associated phenomena.

Citation: Pudasaini, S. P. (2012), A general two-phase debris flow model, *J. Geophys. Res.*, *117*, F03010, doi:10.1029/2011JF002186.

1. Introduction

[2] Debris flows are extremely destructive and dangerous natural hazards. There is a significant need for reliable methods for predicting the dynamics, runout distances, and inundation areas of such events. Debris flows are multi-phase, gravity-driven flows consisting of randomly dispersed interacting phases [*O'Brien et al.*, 1993; *Hutter et al.*, 1996; *Iverson*, 1997; *Iverson and Denlinger*, 2001; *Pudasaini et al.*, 2005; *Takahashi*, 2007; *Hutter and Schneider*, 2010a, 2010b]. They consist of a broad distribution of grain sizes mixed with fluid. The rheology and flow behavior can vary and depend on the sediment composition and percentage of solid and fluid phases. Significant research in the past few decades has focused on single-phase, dry granular avalanches [*Savage and Hutter*, 1989; *Hungr*, 1995; *Hutter et al.*, 1996; *Gray et al.*, 1999; *Pudasaini and Hutter*, 2003; *Zahibo et al.*, 2010], single-phase debris flows [*Bagnold*, 1954; *Chen*, 1988; *O'Brien et al.*, 1993; *Takahashi*, 2007; *Pudasaini*, 2011], flows composed of solid-fluid mixtures [*Iverson*, 1997; *Iverson and Denlinger*, 2001; *Pudasaini et al.*, 2005], two-layer flows [*Fernandez-Nieto et al.*, 2008], and two-fluid debris flows [*Pitman and Le*, 2005]. However, a comprehensive theory accounting for all the interactions between the solid particles and the fluid is still out of reach.

[3] Two-phase granular-fluid mixture flows are characterized primarily by the relative motion and interaction between the solid and fluid phases. Although *Iverson and Denlinger* [2001] and *Pudasaini et al.* [2005] utilized equations that allow basal pore fluid pressure to evolve and include viscous effects, their mixture models are only quasi two-phase or virtually single-phase because they neglect differences between the fluid and solid velocities. Thus, drag force cannot be generated. A key and ad-hoc assumption in *Iverson* [1997], *Iverson and Denlinger* [2001], *Pudasaini et al.* [2005] and *Fernandez-Nieto et al.* [2008] is that the total stress (**T**) can be divided into solid and fluid constituents by introducing a factor Λ_f such that the partial solid and fluid stresses are given by $(1 - \Lambda_f)\mathbf{T}$ and $\Lambda_f\mathbf{T}$, respectively. In these models, Λ_f (ratio between the basal pore fluid pressure and the total basal normal stress, i.e., the pore pressure ratio [see *Hungr*, 1995]) is treated phenomenologically as an internal variable. Also, in these models, volume fraction of the solid is not a dynamical field variable [*Hutter and Schneider*, 2010a, 2010b].

[4] As observed in natural debris flows, the solid and fluid phase velocities may deviate substantially from each other, essentially affecting flow mechanics. Depending on the flow configuration and the material involved, several additional physical mechanics are introduced as mentioned below. Drag is one of the very basic and important mechanisms of two-phase flow as it incorporates coupling between the

[1]Department of Geodynamics and Geophysics, Steinmann Institute, University of Bonn, Bonn, Germany.
[2]Also at School of Science, Kathmandu University, Kathmandu, Nepal.

Corresponding author: S. P. Pudasaini, Department of Geodynamics and Geophysics, Steinmann Institute, University of Bonn, Nussallee 8, D-53115 Bonn, Germany. (pudasaini@geo.uni-bonn.de)

0148-0227/12/2011JF002186

phases. In terms of modeling the relative motion between the solid and the fluid phases and the associated drag, *Pitman and Le* [2005] proposed a two-fluid debris flow model in which both the solid and fluid phases are considered as 'fluids'. The *Pitman and Le* [2005] model was subsequently modified by *Pelanti et al.* [2008], but both models neglect viscous stresses, another important physical aspect of two-phase flows. In *Pitman and Le* [2005] model, the drag force depends on the terminal velocity of a freely falling solid particle through a less dense fluid, and there is no direct effect of fluid viscosity on drag. For the fluid phase, the *Pitman and Le* [2005] model and its variants [*Pelanti et al.*, 2008; *Pailha and Pouliquen*, 2009] retain only a fluid-pressure gradient and neglect the viscous effects of the fluid phase. However, the fluid phase in natural debris flows can deviate substantially from an ideal fluid (pure water, for example, but with negligible viscosity) depending on the constituents forming the fluid phase, which can include silt, clay, and fine particles. In many natural debris flows, viscosity can range from 0.001 to 10 Pas or higher [*Takahashi*, 1991, 2007; *Iverson*, 1997]. A small change in the fluid viscosity may lead to substantial change in the dynamics of the debris motion.

[5] Debris-flow dynamics depend on many different factors, including flow properties, topography, and initial and boundary conditions. Although fluid pressure [*Iverson*, 1997; *Iverson and Denlinger*, 2001; *Pitman and Le*, 2005; *Pudasaini et al.*, 2005], viscous effects [*Iverson*, 1997; *Iverson and Denlinger*, 2001; *Pudasaini et al.*, 2005] and simple drag between the two phases [*Pitman and Le*, 2005] have been included in various models, three important physical aspects often observed in the natural debris flows are not yet included in any models. (*i*) One phase (e.g., solid) may accelerate relative to another phase (e.g., fluid), thus inducing virtual mass. Relative acceleration between the phases is always present [*Ishii*, 1975; *Ishii and Zuber*, 1979; *Drew*, 1983; *Drew and Lahey*, 1987; *Kytoma*, 1991; *Ishii and Hibiki*, 2006; *Kolev*, 2007]. Hence, dynamic modeling and numerical simulation should include virtual mass effects. (*ii*) The amount and gradient of the solid particles considerably influences flow, which can enhance or diminish viscous effects. If the solid-concentration gradient is positive in the flow direction, then the viscous shear-stress will be enhanced by the increased number of solid particles in the downstream direction. Thus, fluid shear stress is enhanced (or suppressed) by the gradient of the volumetric concentration of the solid particles [*Ishii*, 1975; *Drew*, 1983; *Ishii and Hibiki*, 2006], and this effect should be included in dynamic models. (*iii*) Depending on the amount of grains and flow situation, I propose that drag should combine the solid- and fluid-like contributions in a linear (laminar-type, at low velocity) and quadratic (turbulent-type; e.g., Voellmy drag; at high velocity) manner. Here, a *Richardson and Zaki* [1954] relationship between sedimentation velocity and the terminal velocity of an isolated particle falling in a fluid, and the Kozeny-Carman packing of spheres are combined to develop a new generalized drag coefficient that can be applied to a wide range of problems from the simple linear drag to quadratic drag. There are two distinct contributions in the proposed drag force; one fluid-like, and the other solid-like, having different degrees of importance (sections 2.2.1, 6.2, and Appendix A). A generalized drag coefficient, modeled by a linear combination of these two limiting contributions, is presented in this paper. Existing models are limited either to solid-like or to fluid-like drag contribution to flow resistance.

[6] The mathematical structure of equations can also be an important aspect of granular- and debris-flow modeling [*Pudasaini et al.*, 2005; *Pelanti et al.*, 2008]. Dynamical-model equations should be constructed in a standard, and preferably conservative, form. Such a form facilitates numerical integration of model equations even when shocks are formed as has been observed in natural and laboratory flows of debris and granular materials on inclined slopes [*Pudasaini et al.*, 2005, 2007; *Pudasaini and Kröner*, 2008; *Pudasaini*, 2011]. However, the final form of model equations depends largely on how one formulates a model and on how mathematical operators are applied. Here, I start with rigorously structured basic conservation equations, and maintain their structure to the final model expressions. This makes the new model unique, and the most generalized, two-phase mixture mass flow model that exists. Both three-dimensional and depth-averaged, two-dimensional two-phase model equations are presented.

[7] Starting from *Ishii* [1975], *Ishii and Zuber* [1979] and *Drew* [1983], I use phase-averaged mass and momentum balance equations for the solid and fluid components; adopt Mohr-Coulomb plasticity for the solid phase; use a non-Newtonian rheology for the fluid phase; utilize a solid-volume-fraction-gradient-enhanced viscous stress; include virtual mass force due to relative accelerations between the solid and fluid constituents; and introduce a generalized drag coefficient based on *Richardson and Zaki* [1954] and Kozeny-Carman [see, e.g., *Kozeny*, 1927; *Carman*, 1937, 1956; *Kytoma*, 1991; *Ouriemi et al.*, 2009; *Pailha and Pouliquen*, 2009]. I derive a set of well-structured, hyperbolic-parabolic model equations in conservative form [*Pudasaini and Hutter*, 2003, 2007]. The model equations reveal strong coupling between solid and fluid momentum transfer, both through interfacial momentum transfer and the solid-concentration-gradient-enhanced viscous fluid stresses. Furthermore, the virtual-mass forces couple the momentum equations of the two components, which would be only weakly coupled (by the volume fraction of solid) in the absence of drag forces. The model presented unifies the three pioneering theories in geophysical mass flows, the dry granular avalanche model of *Savage and Hutter* [1989], the debris-flow model of *Iverson* [1997] and *Iverson and Denlinger* [2001], and the two-fluid debris-flow model of *Pitman and Le* [2005], and result in a new, generalized two-phase debris-flow model. The generalized model reduces to three special cases which are compared with the three (classical) avalanche and debris-flow models noted above. The similarities and differences between the reduced model and the relatively simple classical models are discussed in detail.

[8] To develop insight into the basic features of the complex governing equations, the new model is applied to simple, one-dimensional debris flows down an inclined channel. The influence of the generalized drag, buoyancy, virtual mass, Newtonian viscous stress and the enhanced non-Newtonian viscous stress on the overall dynamics of a two-phase debris flow is analyzed in detail. Furthermore, the influence of the initial distribution of the solid volume

fraction on the evolution of the solid and fluid constituents, and on the fluid (or the solid) volume fraction is investigated. The simulation results demonstrate fundamentally new features of the proposed model as compared to the classical mixture [*Iverson and Denlinger*, 2001; *Pudasaini et al.*, 2005] and two-fluid [*Pitman and Le*, 2005] models. The results highlight the basic physics associated with the contributions of the viscous stresses (both Newtonian and non-Newtonian), virtual mass, generalized drag, and buoyancy, and thus imply the applicabilities of the new model to a wide range of two-phase geophysical mass flows.

2. Model Derivation

[9] The two phases are characterized by distinct material properties: the fluid phase is characterized by its density ρ_f, viscosity η_f, and isotropic stress distribution; the solid phase is characterized by its density ρ_s, internal and basal friction angles ϕ and δ, and anisotropic stress distribution, K (lateral earth pressure coefficient). These characterizations and the presence of relative motion between phases lead to two different mass and momentum balance equations for the solid and the fluid phases, respectively. Let $\mathbf{u}_s = (u_s, v_s, w_s)$, $\mathbf{u}_f = (u_f, v_f, w_f)$ and α_s, $\alpha_f (= 1 - \alpha_s)$ denote the velocities, and volume fractions for the solid and the fluid constituents, denoted by the suffix s and f, respectively. Following *Ishii* [1975], *Ishii and Zuber* [1979], and *Drew* [1983], I consider the phase-averaged balance equations for mass and momentum conservations, and make the following assumptions: surface tension is negligible; interfacial solid and fluid pressures are identical to the fluid pressure; the solid and fluid components are incompressible; and no phase change occurs.

2.1. Balance Equations for Mass and Momentum

[10] The mass balance equations for the solid and fluid constituents are:

$$\frac{\partial \alpha_s}{\partial t} + \nabla \cdot (\alpha_s \mathbf{u}_s) = 0, \tag{1a}$$

$$\frac{\partial \alpha_f}{\partial t} + \nabla \cdot \left(\alpha_f \mathbf{u}_f\right) = 0. \tag{1b}$$

The momentum equations for the solid and the fluid phases are written in conservative form as

$$\frac{\partial}{\partial t}(\alpha_s \rho_s \mathbf{u}_s) + \nabla \cdot (\alpha_s \rho_s \mathbf{u}_s \otimes \mathbf{u}_s) = \alpha_s \rho_s \mathbf{f} - \nabla \cdot \alpha_s \mathbf{T}_s + p \nabla \alpha_s + \mathbf{M}_s, \tag{2a}$$

$$\frac{\partial}{\partial t}\left(\alpha_f \rho_f \mathbf{u}_f\right) + \nabla \cdot \left(\alpha_f \rho_f \mathbf{u}_f \otimes \mathbf{u}_f\right) = \alpha_f \rho_f \mathbf{f} - \alpha_f \nabla p + \nabla \cdot \alpha_f \boldsymbol{\tau}_f + \mathbf{M}_f, \tag{2b}$$

where $\mathbf{f}$ is the body force density, $-\mathbf{T}_s$ is the negative Cauchy stress tensor (here, for the solid), $\boldsymbol{\tau}_f$ is the extra stress for fluid ($\mathbf{T}_f = -p\mathbf{I} + \boldsymbol{\tau}_f$; $\mathbf{T}_f$ is the Cauchy stress tensor for fluid), $\mathbf{M}$ is the interfacial force density ($\mathbf{M}_s + \mathbf{M}_f = 0$), $p\nabla\alpha_s$ accounts for the buoyant force, and p is the fluid pressure (Appendix B). To quote from *Drew* [1983, pp. 273]: "The reason for this terminology is, of course, that the buoyant force on an object is due to the distribution of the pressure of the surrounding fluid on its boundary." It is important to note that in (2) the solid and fluid stresses are accompanied by the respective solid and fluid volume fractions, α_s and α_f, and that $\mathbf{T}_s$ and $\boldsymbol{\tau}_f$ are not coupled. Furthermore, α_s and α_f appear inside the differential operators, and the inertial and stress terms are in conservative form. With regard to the basic structure of the momentum equations, these are the fundamental differences between the basic mixture momentum equations used by *Iverson* [1997] and *Iverson and Denlinger* [2001], and the phase-averaged equations used by *Anderson and Jackson* [1967] and *Pitman and Le* [2005]. My approach here also differs from that presented by *Pelanti et al.* [2008], who re-wrote the inertial part of the *Pitman and Le* [2005] model in conservative form (structure). However, as shown in *Drew* [1983] and revealed by (2), the rigorous averaging process produces fundamentally different terms on the right-hand sides of the momentum equations as compared to *Pelanti et al.* [2008]. These distinct features of the field equations, and the way I develop and implement the generalized drag, virtual mass, and the solid-volume-fraction-gradient-enhanced non-Newtonian fluid viscous stress, ultimately lead to new model equations in well-structured conservative form.

2.2. Constitutive Equations

[11] Constitutive equations are required for the interfacial force density $\mathbf{M}_s$, the solid stress tensor $\mathbf{T}_s$, and the fluid viscous stress tensor $\boldsymbol{\tau}_f$. Major challenges lie in modeling these terms.

2.2.1. Interfacial Force Density

[12] In the generalized interfacial momentum transfer, $\mathbf{M}_s$, I include the force associated with viscous drag, $\mathbf{M}_D$, on the particulate phase, and the force due to the relative acceleration of the solids with respect to the fluid (virtual mass, $\mathbf{M}_{VM}$):

$$\mathbf{M}_s = \mathbf{M}_D + \mathbf{M}_{VM} = C_{DG}(\mathbf{u}_f - \mathbf{u}_s)|\mathbf{u}_f - \mathbf{u}_s| + C_{VMG}\frac{d}{dt}(\mathbf{u}_f - \mathbf{u}_s), \tag{3}$$

where, C_{DG} is the generalized drag coefficient and C_{VMG} is the generalized virtual mass coefficient.

[13] *Generalized drag force.* The viscous drag, $\mathbf{M}_D$, can be written as $\mathbf{M}_D = \alpha_s \mathbf{F}_D / B_d$, where $\mathbf{F}_D$ is the drag force (B_d is the particle volume), which in classical form reads [*Ishii and Zuber*, 1979]: $\mathbf{F}_D = \frac{1}{2} C_{DG} \rho_f (\mathbf{u}_f - \mathbf{u}_s)|\mathbf{u}_f - \mathbf{u}_s| A_d$, where A_d is the projected area of the particle. Then, by using the steady state, one-dimensional momentum equations, the magnitudes of $\mathbf{F}_D$ and $\mathbf{M}_D$ are obtained [*Ishii*, 1975; *Kolev*, 2007]: $F_D = B_d \alpha_f (\rho_s - \rho_f) g$, $M_D = \alpha_s \alpha_f (\rho_s - \rho_f) g$. This reveals the most basic features of the drag force: $M_D = 0$ if in the limit the solid or fluid volume fraction vanishes ($\alpha_s = 0$ or $\alpha_f = 0$), and if the particles are neutrally buoyant (i.e., $\rho_s - \rho_f = 0$) [*Bagnold*, 1954; *Pudasaini*, 2011].

[14] The generalized drag coefficient, C_{DG} can be written as:

$$C_{DG} = M_D / |\mathbf{u}_f - \mathbf{u}_s|^2 = \alpha_s \alpha_f \left(\rho_s - \rho_f\right) g / |\mathbf{u}_f - \mathbf{u}_s|^2. \tag{4}$$

The mass balances in (1) imply that the total mixture is divergence free, $\nabla \cdot (\alpha_s \mathbf{u}_s + \alpha_f \mathbf{u}_f) = 0$. Thus, the net volume

flux must vanish, $\alpha_s \mathbf{u}_s + \alpha_f \mathbf{u}_f = 0$ [*Pitman and Le*, 2005]. The relative phase velocity $|\mathbf{u}_f - \mathbf{u}_s|$ can be rearranged in terms of the solid and the fluid constituent velocities to get:

$$\left|\mathbf{u}_f - \mathbf{u}_s\right| = \frac{1}{\alpha_s}|\mathbf{u}_f|, \tag{5a}$$

$$\left|\mathbf{u}_f - \mathbf{u}_s\right| = \frac{1}{\alpha_f}|\mathbf{u}_s|. \tag{5b}$$

Consider a parameter $\mathcal{P} \in (0,\ 1)$ which eventually combines the solid-like and fluid-like drag contributions to flow resistance in two-phase debris flows (section 6.2 and Appendix A). Multiply (5a) by $\mathcal{P}$ and (5b) by $(1 - \mathcal{P})$ and add to obtain their linear combination, which when squared leads to a unique expression:

$$|\mathbf{u}_f - \mathbf{u}_s|^2 = \left[\mathcal{P}\frac{1}{\alpha_s}\left|\mathbf{u}_f\right| + (1-\mathcal{P})\frac{1}{\alpha_f}|\mathbf{u}_s|\right]^2. \tag{6}$$

Until this point, only the fluid dynamical equations are used. Now, I approach some experimental results to model $|\mathbf{u}_s|$ and $|\mathbf{u}_f|$.

[15] Consider one-dimensional vertical flows. As in *Richardson and Zaki* [1954] and *Pitman and Le* [2005],

$$|u_s| = \mathcal{U}_s = \alpha_f^M \mathcal{U}_T, \tag{7}$$

where $\mathcal{U}_s$ is the sedimentation velocity of a dispersion of particles in a fluid, and $\mathcal{U}_T$ is the terminal velocity of an isolated particle falling in the fluid. The parameter $M = M(Re_p)$ depends weakly on the particle Reynolds number Re_p, and varies from 4.65 to 2.4 [*Pitman and Le*, 2005]. Equation (7) is mainly applicable for dilute flows where the inter-particle distance is much larger than the particle size.

[16] Next, consider fluid flow through a relatively dense packing of solid grains, similar to the flow of fluid through the porous medium. Typical fluid velocity under such conditions is represented by:

$$\begin{aligned}\left|u_f\right| \approx \mathcal{K} &= \rho_f g \frac{\kappa}{\eta_f} = \frac{\rho_f g}{\eta_f}\alpha_{ck} d^2 = \frac{\rho_f g d^2}{\eta_f}\frac{\alpha_f^3}{180\alpha_s^2} \\ &= \frac{\gamma}{180}\left(\frac{\alpha_f}{\alpha_s}\right)^3 \alpha_s Re_p \mathcal{U}_T,\end{aligned} \tag{8}$$

where, $\mathcal{K}$ is hydraulic conductivity, κ is permeability, α_{ck} is the Kozeny-Carman packing of spheres, d is particle diameter, η_f is fluid viscosity, $\gamma = \rho_f/\rho_s$ is the density ratio, $Re_p = \rho_f d\mathcal{U}_T/\eta_f$ is the particle Reynolds number [see, e.g., *Pailha and Pouliquen*, 2009], and assume that $\mathcal{U}_T = \sqrt{gd/\gamma}$, which is an approximation for particle falling through a non-dense fluid medium. Combining (4), (6), (7) and (8) I obtain a new generalized drag coefficient:

$$C_{DG} = \frac{\alpha_s \alpha_f \left(\rho_s - \rho_f\right) g}{\left[\mathcal{U}_T\left\{\mathcal{P}\mathcal{F}\left(Re_p\right) + (1-\mathcal{P})\mathcal{G}\left(Re_p\right)\right\}\right]^{\jmath}}, \tag{9}$$

where $\mathcal{F} = \gamma\left(\alpha_f/\alpha_s\right)^3 Re_p/180$ and $\mathcal{G} = \alpha_f^{M\left(Re_p\right)-1}$. $\mathcal{F}$ depends linearly on the particle Reynolds number, density ratio and the cube power of the ratio between fluid and solid volume fractions. However, $\mathcal{G}$ only depends weakly on the fluid volume fraction and the particle Reynolds number. Furthermore, $\jmath = 1$ or 2 should be selected according to whether simple linear (laminar-type, at low velocity) or quadratic (turbulent-type; e.g., Voellmy drag; at high velocity) drag coefficients are considered. The parameter $\mathcal{P}$ can play a crucial role to fit the data and the model calibration.

[17] It is important to mention that in practical applications, the value of C_{DG} is usually set to some numerical value that optimizes the fit between observations and numerical simulations (where $C_{DG} = 0.022$ is used) [see, e.g., *Zwinger et al.*, 2003]. However, here I propose that this drag coefficient be expressed explicitly in terms of essential physical parameters, for example, the volume fractions of the solid and fluid, the solid and fluid densities, terminal velocity of solid particles, particle diameter, and fluid viscosity. $\mathcal{F}$ represents fluid flow through a solid skeleton (e.g., granular-rich debris flows) [see, *Takahashi*, 2007], whereas $\mathcal{G}$ represents solid particles moving through fluid (e.g., particle-laden flows). $\mathcal{F}$ and $\mathcal{G}$ may have different degrees of importance depending on the nature of the flow. Therefore, the generalized drag coefficient is modeled by a linear combination of these contributions. There are two limiting cases: $\mathcal{P} = 0$ is more suitable when solid particles are moving through a fluid. In contrast, $\mathcal{P} = 1$ is more suitable for flows of fluids through dense packings of grains [*Kytoma*, 1991; *Pitman and Le*, 2005; *Ouriemi et al.*, 2009; *Pailha and Pouliquen*, 2009]. The proposed generalized drag coefficient offers the opportunity to simulate a wide spectrum of flows. By setting $\mathcal{P} = 0$ and $\jmath = 1$, one recovers the drag coefficient of *Pitman and Le* [2005], and $\mathcal{P} = 1$ and $\jmath = 1$ corresponds to the drag coefficient in *Pailha and Pouliquen* [2009]. See the Appendix A for detailed discussion on the drag.

[18] *Virtual mass.* The proposed drag force includes the interaction between fluid and solids in uniform flow fields under nonaccelerating conditions. In reality, the solid particles may accelerate relative to the fluid. In this situation, part of the ambient fluid is also accelerated. This induces an additional force contribution in the flow, which is called the added mass force or virtual mass force. A simple way of realizing virtual mass force is by considering the change in kinetic energy of the fluid surrounding an accelerating particle. The virtual mass coefficient depends on the volume fraction of the solid. Following *Ishii* [1975], *Ishii and Zuber* [1979], *Drew* [1983] and *Drew and Lahey* [1987], the coefficients of the generalized virtual mass (C_{VMG}), and the virtual mass (C_{VM}) are defined as

$$C_{VMG} = \alpha_s \rho_f C_{VM}(\alpha_s), \quad C_{VM}(\alpha_s) = 0.5(1 + 2\alpha_s)/\alpha_f. \tag{10}$$

[19] For small values of α_s, $C_{VM} \approx 0.5$ [*Maxey and Riley*, 1993]. For unsteady, inviscid flow *Rivero et al.* [1991] also showed $C_{VM} \approx 0.5$. For practical purposes, C_{VM} can also be assumed constant, or at least independent of flow depth. The convective derivative $d(\mathbf{u}_f - \mathbf{u}_s)/dt$, which is required for virtual mass, can be written in many different ways. Here, I use the simple expression as suggested by *Lyczkowski et al.* [1978]:

$$\frac{d}{dt}\left(\mathbf{u}_f - \mathbf{u}_s\right) = \frac{d\mathbf{u}_f}{dt} - \frac{d\mathbf{u}_s}{dt} = \left(\frac{\partial \mathbf{u}_f}{\partial t} + \mathbf{u}_f \cdot \nabla \mathbf{u}_f\right) - \left(\frac{\partial \mathbf{u}_s}{\partial t} + \mathbf{u}_s \cdot \nabla \mathbf{u}_s\right). \tag{11}$$

These expressions will be united with the inertial part of (2). Special attention should be paid as these expressions do not include the volume fraction of the solid inside the derivatives. All previous geophysical mass flow models [*Iverson and Denlinger*, 2001; *Pitman and Le*, 2005; *Pudasaini et al.*, 2005; *Pelanti et al.*, 2008] neglect virtual mass effect.

2.2.2. Stresses

[20] *Solid stresses.* Following prior considerations [*Savage and Hutter*, 1989; *Gray et al.*, 1999; *Pudasaini and Hutter*, 2003, 2007], solid stresses are assumed to satisfy the Mohr-Coulomb plasticity criterion. The Cauchy stress components are expressed in terms of the normal pressure (stress) and an earth-pressure coefficient:

$$|\mathbf{S}| = N\tan\phi, \quad T_{xx} = K_x T_{zz}, \quad T_{yy} = K_y T_{zz}, \tag{12}$$

where $\mathbf{S}$ is the shear stress, N is the normal pressure on any plane element, and K is the earth-pressure coefficient. See Appendix B for alternative solid stress closures.

[21] *Fluid extra stresses.* Following *Ishii* [1975], *Drew* [1983], and *Ishii and Hibiki* [2006], the phase-averaged viscous-fluid stresses are modeled using a non-Newtonian fluid rheology:

$$\boldsymbol{\tau}_f = \eta_f\left[\nabla\mathbf{u}_f + \left(\nabla\mathbf{u}_f\right)^t\right] - \eta_f\frac{\mathcal{A}(\alpha_f)}{\alpha_f} \cdot\left[(\nabla\alpha_s)\left(\mathbf{u}_f - \mathbf{u}_s\right) + \left(\mathbf{u}_f - \mathbf{u}_s\right)(\nabla\alpha_s)\right]. \tag{13}$$

Here, $\mathcal{A}(\alpha_f)$ is called the mobility of the fluid at the interface. As $\alpha_s \to 0$, $\mathcal{A} \approx 1$, implying perfect mobility (means fluid moves without the disturbance of solid particles). Imagine the situation in which the solid particles are moving faster than the fluid. If the solid-concentration gradient is zero (uniform distribution of solid particles), then the fluid viscous-stress does not experience any additional disturbance. If the concentration gradient is positive, then the viscous shear-stress will be enhanced by the presence of an increasing number of solid particles in the downstream direction. In contrast, a negative solid-concentration gradient means that the number of particles is decreasing in the downstream direction, thus reducing the fluid viscous stress. This is intuitively clear as far as the debris flows, particle laden flows, and dispersive particle flows are concerned. To my knowledge, such a potentially important effect of the solid-concentration gradient on the viscous stress of the fluid has not yet been modeled, explored experimentally or simulated in the context of the geophysical mass flows. Therefore, $\mathcal{A}$ can be treated as a phenomenological parameter. In previous mixture models [*Iverson and Denlinger*, 2001; *Pudasaini et al.*, 2005] concentration gradients are neglected, and the relative motion of solids with respect to the fluid is also neglected. In prior models, the fluid effect is incorporated as an internal variable for the basal fluid pressure. Existing two-fluid models [*Pitman and Le*, 2005; *Pelanti et al.*, 2008; *Pailha and Pouliquen*, 2009] neglect the fluid shear stress $\boldsymbol{\tau}_f$, and only hydrostatic fluid pressure is retained (in *Pailha and Pouliquen* [2009] pressure is modified to include a granular dilatational effect). It is important to realize that in (13) the fluid shear stress is enhanced (or reduced) by the gradient of the solids concentration. Note that, $\eta_f\left[\nabla\mathbf{u}_f + \left(\nabla\mathbf{u}_f\right)^t\right]$ is the Newtonian viscous stress, and $\eta_f\frac{\mathcal{A}(\alpha_f)}{\alpha_f}\left[(\nabla\alpha_s)\left(\mathbf{u}_f - \mathbf{u}_s\right) + \left(\mathbf{u}_f - \mathbf{u}_s\right)(\nabla\alpha_s)\right]$ is a Non-Newtonian viscous stress that depends on the solid-volume-fraction gradient $\nabla\alpha_s$, which enhances the apparent viscous stress, $\boldsymbol{\tau}_f$.

3. A Three-Dimensional Two-Phase Debris-Flow Model

[22] Collecting the mass and momentum balance equations, the interfacial momentum transfer, and the solid and fluid stress expressions from (1)–(3), (9)–(13), the three-dimensional two-phase debris flow model can be written as:

$$\frac{\partial\alpha_s}{\partial t} + \nabla\cdot(\alpha_s\mathbf{u}_s) = 0, \tag{14a}$$

$$\frac{\partial\alpha_f}{\partial t} + \nabla\cdot\left(\alpha_f\mathbf{u}_f\right) = 0, \tag{14b}$$

$$\frac{\partial}{\partial t}(\alpha_s\rho_s\mathbf{u}_s) + \nabla\cdot(\alpha_s\rho_s\mathbf{u}_s\otimes\mathbf{u}_s) = \alpha_s\rho_s\mathbf{f} - \nabla\cdot\alpha_s\mathbf{T}_s + p\nabla\alpha_s + \mathbf{M}_s, \tag{14c}$$

$$\frac{\partial}{\partial t}\left(\alpha_f\rho_f\mathbf{u}_f\right) + \nabla\cdot\left(\alpha_f\rho_f\mathbf{u}_f\otimes\mathbf{u}_f\right) = \alpha_f\rho_f\mathbf{f} - \alpha_f\nabla p + \nabla\cdot\alpha_f\boldsymbol{\tau}_f + \mathbf{M}_f, \tag{14d}$$

where,

$$\mathbf{M}_s = \frac{\alpha_s\alpha_f\left(\rho_s - \rho_f\right)g}{\left[\mathcal{U}_T\left\{\mathcal{P}\mathcal{F}(Re_p) + (1-\mathcal{P})\mathcal{G}(Re_p)\right\}\right]^J}\left(\mathbf{u}_f - \mathbf{u}_s\right)|\mathbf{u}_f - \mathbf{u}_s|^{J-1} + \frac{1}{2}\alpha_s\rho_f\left(\frac{1+2\alpha_s}{\alpha_f}\right)\left[\left(\frac{\partial\mathbf{u}_f}{\partial t} + \mathbf{u}_f\cdot\nabla\mathbf{u}_f\right) - \left(\frac{\partial\mathbf{u}_s}{\partial t} + \mathbf{u}_s\cdot\nabla\mathbf{u}_s\right)\right], \tag{14e}$$

$$|\mathbf{S}| = N\tan\phi, \quad T_{xx} = K_x T_{zz}, \quad T_{yy} = K_y T_{zz}, \tag{14f}$$

$$\boldsymbol{\tau}_f = \eta_f\left[\nabla\mathbf{u}_f + \left(\nabla\mathbf{u}_f\right)^t\right] - \eta_f\frac{\mathcal{A}(\alpha_f)}{\alpha_f} \cdot\left[(\nabla\alpha_s)\left(\mathbf{u}_f - \mathbf{u}_s\right) + \left(\mathbf{u}_f - \mathbf{u}_s\right)(\nabla\alpha_s)\right], \tag{14g}$$

and $\mathbf{M}f = -\mathbf{M}_s$. There is strong coupling between the solid and the fluid momentum transfer both through the interfacial momentum transfer $\mathbf{M}$, which includes the viscous drag and the virtual mass force, and the enhanced non-Newtonian viscous fluids stresses. In (14), there are 8 equations and 8 unknowns (u_s, v_s, w_s; u_f, v_f, w_f; α_s, p). The system is closed and can be solved numerically.

4. A Reduced Two-Dimensional Two-Phase Debris Flow Model

[23] Three-dimensional model (equations 14) typically are unmanageable or demand huge computational efforts when applied to natural-scale geophysical mass flows, which can involve masses as large as 10^6 to 10^{13} m^3 [*Legros*, 2002; *Crosta et al.*, 2004; *Strom and Korup*, 2006; *Pudasaini and Hutter*, 2007; *Sosio et al.*, 2008]. One way to make the problem more tractable is to assume that flows are long (or wide) relative to their depth, and to use depth-averaging in the z direction. Thus, I develop a set of depth-averaged equations for the flowing mass and momentum transfer for the solid and fluid components. This involves a sequence of

processes that rigorously transform the three-dimensional equations into a relatively simple set of equations.

4.1. Scaling Analysis

[24] The scaling analysis is performed with the equations: $(x,\ y,\ z,\ F,\ t) = \left(L\hat{x}, L\hat{y}, H\hat{z}, H\hat{F}, \sqrt{L/g}\hat{t}\right)$, $(u,\ v,\ w) = \sqrt{gL}(\hat{u}, \hat{v}, \varepsilon\hat{w})$, $(T_{xx},\ T_{yy},\ T_{zz}) = \rho_s gH\left(\hat{T}_{xx}, \hat{T}_{yy}, \hat{T}_{zz}\right)$, $(T_{xy},\ T_{xz},\ T_{yz}) = \rho_s gH\mu\left(\hat{T}_{xy}, \hat{T}_{xz}, \hat{T}_{yz}\right), p = \rho_f gH\hat{p}$ [*Iverson*, 1997; *Pitman and Le*, 2005; *Pudasaini and Hutter*, 2007], where L and H are the typical extent and depth of debris flow, $\varepsilon = H/L$ is the aspect ratio, F is a scalar function, and $\mu = \tan\delta$ is the basal friction coefficient. The scaling for solid stresses is introduced in accordance with Coulomb rheology (normal and shear stresses are scaled with $\rho_s gH$ and $\mu\rho_s gH$). For notational brevity, the hats are dropped from the respective terms and it is realized that all the field variables are non-dimensional. Using the defined scaling equations, (14c)–(14d) can be written in non-dimensional form. With some algebraic manipulations, the virtual mass terms can be combined with the inertial terms. Then, solid-phase x, y and z momentum equations (14c), respectively, yield (where, $\mathbf{T} = \mathbf{T}_s$ is solid stress tensor, $\mathcal{C} = C_{VM}$ is virtual mass coefficient, $\tilde{\mathcal{C}} = \left(\alpha_s/\alpha_f\right)\mathcal{C}$ is volume fraction ratio weighted virtual mass coefficient)

$$
\begin{aligned}
&(1+\gamma\mathcal{C})\left[\frac{\partial}{\partial t}(\alpha_s u_s) + \frac{\partial}{\partial x}\left(\alpha_s u_s^2\right) + \frac{\partial}{\partial y}(\alpha_s u_s v_s) + \frac{\partial}{\partial z}(\alpha_s u_s w_s)\right]\\
&\quad - \gamma\tilde{\mathcal{C}}\left[\frac{\partial}{\partial t}(\alpha_f u_f) + \frac{\partial}{\partial x}\left(\alpha_f u_f^2\right) + \frac{\partial}{\partial y}(\alpha_f u_f v_f) + \frac{\partial}{\partial z}(\alpha_f u_f w_f)\right]\\
&= \alpha_s g^x - \left\{\varepsilon\frac{\partial}{\partial x}(\alpha_s T_{xx}) + \varepsilon\mu\frac{\partial}{\partial y}(\alpha_s T_{xy}) + \mu\frac{\partial}{\partial z}(\alpha_s T_{xz})\right\} + \varepsilon\gamma p\frac{\partial\alpha_s}{\partial x}\\
&\quad + \frac{\alpha_s\alpha_f(1-\gamma)}{\left[\varepsilon\ \mathcal{U}_T\left\{\mathcal{PF}(Re_p) + (1-\mathcal{P})\mathcal{G}(Re_p)\right\}\right]^J}(u_f - u_s)|\mathbf{u}_f - \mathbf{u}_s|^{J-1},
\end{aligned}
\tag{15}
$$

$$
\begin{aligned}
&(1+\gamma\mathcal{C})\left[\frac{\partial}{\partial t}(\alpha_s v_s) + \frac{\partial}{\partial x}(\alpha_s u_s v_s) + \frac{\partial}{\partial y}\left(\alpha_s v_s^2\right) + \frac{\partial}{\partial z}(\alpha_s v_s w_s)\right]\\
&\quad - \gamma\tilde{\mathcal{C}}\left[\frac{\partial}{\partial t}(\alpha_f v_f) + \frac{\partial}{\partial x}(\alpha_f u_f v_f) + \frac{\partial}{\partial y}\left(\alpha_f v_f^2\right) + \frac{\partial}{\partial z}(\alpha_f v_f w_f)\right]\\
&= \alpha_s g^y - \left\{\varepsilon\mu\frac{\partial}{\partial x}(\alpha_s T_{yx}) + \varepsilon\frac{\partial}{\partial y}(\alpha_s T_{yy}) + \mu\frac{\partial}{\partial z}(\alpha_s T_{yz})\right\} + \varepsilon\gamma p\frac{\partial\alpha_s}{\partial y}\\
&\quad + \frac{\alpha_s\alpha_f(1-\gamma)}{\left[\varepsilon\ \mathcal{U}_T\left\{\mathcal{PF}(Re_p) + (1-\mathcal{P})\mathcal{G}(Re_p)\right\}\right]^J}(v_f - v_s)|\mathbf{u}_f - \mathbf{u}_s|^{J-1},
\end{aligned}
\tag{16}
$$

$$
\begin{aligned}
&\varepsilon(1+\gamma\mathcal{C})\left[\frac{\partial}{\partial t}(\alpha_s w_s) + \frac{\partial}{\partial x}(\alpha_s u_s w_s) + \frac{\partial}{\partial y}(\alpha_s v_s w_s) + \frac{\partial}{\partial z}\left(\alpha_s w_s^2\right)\right]\\
&\quad - \varepsilon\gamma\tilde{\mathcal{C}}\left[\frac{\partial}{\partial t}(\alpha_f w_f) + \frac{\partial}{\partial x}(\alpha_f u_f w_f) + \frac{\partial}{\partial y}(\alpha_f v_f w_f) + \frac{\partial}{\partial z}\left(\alpha_f w_f^2\right)\right]\\
&= \alpha_s g^z - \left\{\varepsilon\mu\frac{\partial}{\partial x}(\alpha_s T_{zx}) + \varepsilon\mu\frac{\partial}{\partial y}(\alpha_s T_{zy}) + \frac{\partial}{\partial z}(\alpha_s T_{zz})\right\} + \gamma p\frac{\partial\alpha_s}{\partial z}\\
&\quad + \frac{\alpha_s\alpha_f(1-\gamma)}{\left[\varepsilon^{(J-1)/J}\mathcal{U}_T\left\{\mathcal{PF}(Re_p) + (1-\mathcal{P})\mathcal{G}(Re_p)\right\}\right]^J}(w_f - w_s)|\mathbf{u}_f - \mathbf{u}_s|^{J-1}.
\end{aligned}
\tag{17}
$$

Here, g^x, g^y, g^z are the (non-dimensional) components of gravitational acceleration. Here, I focus on the mechanics of two-phase flows across a locally inclined Cartesian-type topography [*Pitman and Le*, 2005] in which the detailed basal topographic effects can be included in the gradients of the basal topography in x and y-directions, respectively [*Fischer et al.*, 2012].

[25] Similarly, the non-dimensionalized fluid momentum equations (14d), take the form

$$
\begin{aligned}
&(1+\tilde{\mathcal{C}})\left[\frac{\partial}{\partial t}(\alpha_f u_f) + \frac{\partial}{\partial x}\left(\alpha_f u_f^2\right) + \frac{\partial}{\partial y}(\alpha_f u_f v_f) + \frac{\partial}{\partial z}(\alpha_f u_f w_f)\right]\\
&\quad - \mathcal{C}\left[\frac{\partial}{\partial t}(\alpha_s u_s) + \frac{\partial}{\partial x}\left(\alpha_s u_s^2\right) + \frac{\partial}{\partial y}(\alpha_s u_s v_s) + \frac{\partial}{\partial z}(\alpha_s u_s w_s)\right]\\
&= \alpha_f g^x + \varepsilon\left[-\alpha_f\frac{\partial p}{\partial x} + \left\{2\frac{\partial}{\partial x}\left(\frac{1}{N_R}\frac{\partial u_f}{\partial x}\right) + \frac{\partial}{\partial y}\left(\frac{1}{N_R}\left(\frac{\partial u_f}{\partial y} + \frac{\partial v_f}{\partial x}\right)\right)\right.\right.\\
&\quad \left.+ \frac{\partial}{\partial z}\left(\frac{1}{\varepsilon^2 N_R}\frac{\partial u_f}{\partial z} + \frac{1}{N_R}\frac{\partial w_f}{\partial x}\right)\right\} + \left\{2\frac{\partial}{\partial x}\left(\frac{1}{N_{R_A}}\frac{\partial\alpha_s}{\partial x}(u_s - u_f)\right)\right.\\
&\quad + \frac{\partial}{\partial y}\left(\frac{1}{N_{R_A}}\left(\frac{\partial\alpha_s}{\partial x}(v_s - v_f) + \frac{\partial\alpha_s}{\partial y}(u_s - u_f)\right)\right)\\
&\quad \left.\left.+ \frac{\partial}{\partial z}\left(\frac{1}{\varepsilon^2 N_{R_A}}\frac{\partial\alpha_s}{\partial z}(u_s - u_f) + \frac{1}{N_{R_A}}\frac{\partial\alpha_s}{\partial x}(w_s - w_f)\right)\right\}\right]\\
&\quad - \frac{1}{\gamma}\frac{\alpha_s\alpha_f(1-\gamma)}{\left[\varepsilon\ \mathcal{U}_T\left\{\mathcal{PF}(Re_p) + (1-\mathcal{P})\mathcal{G}(Re_p)\right\}\right]^J}(u_f - u_s)|\mathbf{u}_f - \mathbf{u}_s|^{J-1},
\end{aligned}
\tag{18}
$$

$$
\begin{aligned}
&(1+\tilde{\mathcal{C}})\left[\frac{\partial}{\partial t}(\alpha_f v_f) + \frac{\partial}{\partial x}(\alpha_f u_f v_f) + \frac{\partial}{\partial y}\left(\alpha_f v_f^2\right) + \frac{\partial}{\partial z}(\alpha_f v_f w_f)\right]\\
&\quad - \mathcal{C}\left[\frac{\partial}{\partial t}(\alpha_s v_s) + \frac{\partial}{\partial x}(\alpha_s u_s v_s) + \frac{\partial}{\partial y}\left(\alpha_s v_s^2\right) + \frac{\partial}{\partial z}(\alpha_s v_s w_s)\right]\\
&= \alpha_f g^y + \varepsilon\left[-\alpha_f\frac{\partial p}{\partial y} + \left\{\frac{\partial}{\partial x}\left(\frac{1}{N_R}\left(\frac{\partial v_f}{\partial x} + \frac{\partial u_f}{\partial y}\right)\right) + 2\frac{\partial}{\partial y}\left(\frac{1}{N_R}\frac{\partial v_f}{\partial y}\right)\right.\right.\\
&\quad \left.+ \frac{\partial}{\partial z}\left(\frac{1}{N_R}\frac{\partial w_f}{\partial y} + \frac{1}{\varepsilon^2 N_R}\frac{\partial v_f}{\partial z}\right)\right\} + \left\{\frac{\partial}{\partial x}\left(\frac{1}{N_{R_A}}\left(\frac{\partial\alpha_s}{\partial x}(v_s - v_f)\right.\right.\right.\\
&\quad \left.\left.+ \frac{\partial\alpha_s}{\partial y}(u_s - u_f)\right)\right) + 2\frac{\partial}{\partial y}\left(\frac{1}{N_{R_A}}\frac{\partial\alpha_s}{\partial y}(v_s - v_f)\right)\\
&\quad \left.\left.+ \frac{\partial}{\partial z}\left(\frac{1}{N_{R_A}}\frac{\partial\alpha_s}{\partial y}(w_s - w_f) + \frac{1}{\varepsilon^2 N_{R_A}}\frac{\partial\alpha_s}{\partial z}(v_s - v_f)\right)\right\}\right]\\
&\quad - \frac{1}{\gamma}\frac{\alpha_s\alpha_f(1-\gamma)}{\left[\varepsilon\ \mathcal{U}_T\left\{\mathcal{PF}(Re_p) + (1-\mathcal{P})\mathcal{G}(Re_p)\right\}\right]^J}(v_f - v_s)|\mathbf{u}_f - \mathbf{u}_s|^{J-1},
\end{aligned}
\tag{19}
$$

$$
\begin{aligned}
&\varepsilon(1+\tilde{\mathcal{C}})\left[\frac{\partial}{\partial t}(\alpha_f w_f) + \frac{\partial}{\partial x}(\alpha_f u_f w_f) + \frac{\partial}{\partial y}(\alpha_f v_f w_f) + \frac{\partial}{\partial z}\left(\alpha_f w_f^2\right)\right]\\
&\quad - \varepsilon\mathcal{C}\left[\frac{\partial}{\partial t}(\alpha_s w_s) + \frac{\partial}{\partial x}(\alpha_s u_s w_s) + \frac{\partial}{\partial y}(\alpha_s v_s w_s) + \frac{\partial}{\partial z}\left(\alpha_s w_s^2\right)\right]\\
&= \alpha_f g^z - \alpha_f\frac{\partial p}{\partial z} + \varepsilon^2\left[\frac{\partial}{\partial x}\left(\frac{1}{N_R}\frac{\partial w_f}{\partial x}\right) + \frac{\partial}{\partial y}\left(\frac{1}{N_R}\frac{\partial w_f}{\partial y}\right)\right.\\
&\quad \left.+ \frac{\partial}{\partial x}\left(\frac{1}{N_{R_A}}\frac{\partial\alpha_s}{\partial x}(w_s - w_f)\right) + \frac{\partial}{\partial y}\left(\frac{1}{N_{R_A}}\frac{\partial\alpha_s}{\partial y}(w_s - w_f)\right)\right]\\
&\quad + \left[\left\{\frac{\partial}{\partial x}\left(\frac{1}{N_R}\frac{\partial u_f}{\partial z}\right) + \frac{\partial}{\partial y}\left(\frac{1}{N_R}\frac{\partial v_f}{\partial z}\right) + 2\frac{\partial}{\partial z}\left(\frac{1}{N_R}\frac{\partial w_f}{\partial z}\right)\right\}\right.\\
&\quad + \left\{\frac{\partial}{\partial x}\left(\frac{1}{N_{R_A}}\frac{\partial\alpha_s}{\partial z}(u_s - u_f)\right) + \frac{\partial}{\partial y}\left(\frac{1}{N_{R_A}}\frac{\partial\alpha_s}{\partial z}(v_s - v_f)\right)\right.\\
&\quad \left.\left.+ 2\frac{\partial}{\partial z}\left(\frac{1}{N_{R_A}}\frac{\partial\alpha_s}{\partial z}(w_s - w_f)\right)\right\}\right] - \frac{1}{\gamma}\\
&\quad \cdot\frac{\alpha_s\alpha_f(1-\gamma)}{\left[\varepsilon^{(J-1)/J}\ \mathcal{U}_T\left\{\mathcal{PF}(Re_p) + (1-\mathcal{P})\mathcal{G}(Re_p)\right\}\right]^J}(w_f - w_s)|\mathbf{u}_f - \mathbf{u}_s|^{J-1},
\end{aligned}
\tag{20}
$$

where $N_R = \sqrt{gL}\rho_f H/\alpha_f\eta_f$ and $N_{R_A} = \sqrt{gL}\rho_f H/\mathcal{A}\eta_f$ are quasi-Reynolds numbers. The expressions N_R and N_{R_A} are associated with the Newtonian and non-Newtonian viscous stresses, respectively, and N_{R_A} is called the mobility Reynolds number. In the special case in which $\mathcal{A} = \alpha_f$, these quasi-Reynolds numbers coincide. In *Iverson and Denlinger* [2001] and *Pudasaini et al.* [2005], N_{R_A} did not appear. Also, previously in those models only ρ, the debris bulk density, rather than ρ_f appeared in N_R. Here, these quasi-Reynolds numbers are manifestations of the dynamics of the fluid component, in contrast to the mixture models in which N_R is related to the dynamics of bulk debris. The above discussion also implies that there are fundamental differences between the model derived here and the models of *Iverson and Denlinger* [2001] and *Pudasaini et al.* [2005]. Note that, as in *Pitman and Le* [2005], the different scalings with respect to the solid and fluid densities have produced phase-interaction terms (drag) differing by a factor $1/\gamma$.

[26] One of the important aspects of the shallow-flow approximation is to analyze the flow dynamical effect on (fluid) pressure. By neglecting terms of $O(\varepsilon)$ or higher in (20), one obtains

$$\begin{aligned}\alpha_f\frac{\partial p}{\partial z} = \alpha_f g^z + \Bigg[\frac{1}{N_R}\Bigg\{\frac{\partial}{\partial x}\left(\frac{\partial u_f}{\partial z}\right) + \frac{\partial}{\partial y}\left(\frac{\partial v_f}{\partial z}\right) + 2\frac{\partial}{\partial z}\left(\frac{\partial w_f}{\partial z}\right)\Bigg\} \\ + \frac{1}{N_{R_A}}\Bigg\{\frac{\partial}{\partial x}\left(\frac{\partial \alpha_s}{\partial z}\left(u_s - u_f\right)\right) + \frac{\partial}{\partial y}\left(\frac{\partial \alpha_s}{\partial z}\left(v_s - v_f\right)\right) \\ + 2\frac{\partial}{\partial z}\left(\frac{\partial \alpha_s}{\partial z}\left(w_s - w_f\right)\right)\Bigg\}\Bigg] \\ - \frac{1}{\gamma}\frac{\alpha_s\alpha_f(1-\gamma)}{\left[\varepsilon^{(J-1)/J}\ \mathcal{U}_T\left\{\mathcal{PF}\left(Re_p\right) + (1-\mathcal{P})\mathcal{G}\left(Re_p\right)\right\}\right]^J} \\ \cdot \left(w_f - w_s\right)|\mathbf{u}_f - \mathbf{u}_s|^{J-1}. \end{aligned} \tag{21}$$

The terms associated with $1/N_R$ can be re-written as $\frac{\partial}{\partial z}\left(\frac{\partial u_f}{\partial x} + \frac{\partial v_f}{\partial y} + \frac{\partial w_f}{\partial z}\right) + \frac{\partial^2 w_f}{\partial z^2}$. If the debris is moving as a bulk flow without phase-interaction [*Iverson*, 1997; *Iverson and Denlinger*, 2001; *Pudasaini et al.*, 2005], then due to the divergence-free vector field the expression in the bracket would vanish. If we assume $\partial w_f/\partial z \approx 0$ (compatible with the shallow-flow assumption) then the entire expression vanishes. Hence, since the terms associated with $1/N_{R_A}$ and drag do not appear in those bulk mixture models, the fluid pressure is simply hydrostatic. In the model presented here, fluid pressure is not simply hydrostatic, because only the total debris mixture is divergence free, and not the separate components. For simplicity, here I assume that the terms associated with w can be neglected. Then the pressure expression (21) becomes:

$$\begin{aligned}\frac{\partial p}{\partial z} = g^z + \frac{1}{\alpha_f}\Bigg[\frac{1}{N_R}\Bigg\{\frac{\partial}{\partial x}\left(\frac{\partial u_f}{\partial z}\right) + \frac{\partial}{\partial y}\left(\frac{\partial v_f}{\partial z}\right)\Bigg\} \\ + \frac{1}{N_{R_A}}\Bigg\{\frac{\partial}{\partial x}\left(\frac{\partial \alpha_s}{\partial z}\left(u_s - u_f\right)\right) + \frac{\partial}{\partial y}\left(\frac{\partial \alpha_s}{\partial z}\left(v_s - v_f\right)\right)\Bigg\}\Bigg]. \end{aligned} \tag{22}$$

[27] In general, fluid pressure is not hydrostatic in a two-phase flow. A relation similar to (21) is also derived by *Pailha and Pouliquen* [2009], in which a fluid pressure gradient is dependent on drag. If dilation is neglected, as is done here by assuming $w \sim 0$, the drag effect vanishes and fluid pressure is hydrostatic in *Pailha and Pouliquen* [2009]. A non-hydrostatic pressure, such as (22), is incorporated into a debris flow and avalanche model for the first time, which here includes both the dynamics of fluid motion and solid-concentration gradient. For simplicity, following *Iverson and Denlinger* [2001], *Pitman and Le* [2005], *Pudasaini et al.* [2005], *Fernandez-Nieto et al.* [2008], and *Pelanti et al.* [2008], only hydrostatic fluid pressure is considered, $\partial p/\partial z = g^z$, which is justified when N_R and N_{R_A} are much larger than the numerical values of the gradients of velocities and solid volume fractions associated with these terms in (22). Starting with a sufficiently small apparent fluid velocity and a linear Darcy drag, *George and Iverson* [2011] developed a model for a non-hydrostatic pore fluid pressure in a bulk debris mixture that evolves in time as a function of basal pore pressure. However, as mentioned by these authors, such a drag "may oversimplify the effects of complex phase-interaction forces in debris flow".

[28] By neglecting the terms of $O(\varepsilon)$, and assuming weak dependence of α_s with z, (17) yields

$$\begin{aligned}\frac{\partial}{\partial z}(\alpha_s T_{zz}) = \alpha_s g^z + \gamma p\frac{\partial \alpha_s}{\partial z} = \alpha_s g^z - \gamma\alpha_s\frac{\partial p}{\partial z} + \gamma\left[\alpha_s\frac{\partial p}{\partial z} + p\frac{\partial \alpha_s}{\partial z}\right] \\ \approx (1-\gamma)\alpha_s\frac{\partial p}{\partial z} + \left[\gamma\alpha_s^2\frac{\partial}{\partial z}\left(\frac{p}{\alpha_s}\right)\right]. \end{aligned} \tag{23}$$

Because $\alpha_s < 1$, $\alpha_s^2 \ll 1$, and because $\gamma < 1$, $\gamma\alpha_s^2 \approx 0$. In a fully saturated debris flow, $\alpha_s \approx 0.6$ [*Pailha and Pouliquen*, 2009]. In a more fluid-rich debris flow the solids concentration may be stratified. Near the base, α_s may be below 0.6, and at the free-surface, α_s may vanish. For dilute flows, I assume $\alpha_s \approx 0.3$ to be a good approximation of the mean solids concentration. Considering typical solid and fluid densities, $\gamma \approx 0.3$ for natural debris flows. As a result, $\gamma\alpha_s^2$ is about an order of magnitude less than $(1-\gamma)\alpha_s$. This suggests terms in $\gamma\alpha_s^2$ can be disregarded, in which case (23) reduces to

$$\frac{\partial}{\partial z}(\alpha_s T_{zz}) \approx (1-\gamma)\alpha_s\frac{\partial p}{\partial z}. \tag{24}$$

Equation (23) also shows that if fluid pressure and the solid volume fraction vary linearly with depth, this also leads to (24) which is a buoyancy-reduced normal stress acting on the solids. Note that, equations similar to (23)–(24) can also be derived for x and y directions.

4.2. Boundary Conditions

[29] As for single-phase [*Savage and Hutter*, 1989] or mixture flows [*Iverson and Denlinger*, 2001; *Pudasaini et al.*, 2005], or two-fluid flows [*Pitman and Le*, 2005; *Fernandez-Nieto et al.*, 2008], I assume that the solid-fluid mixture, and the solid- and fluid-phase constituents separately satisfy the kinematic free-surface and the bottom boundary conditions. The top surface is traction-free, and Coulomb sliding (for solid) and no-slip (for fluid) conditions are satisfied at the flow base [*Iverson and Denlinger*, 2001; *Pudasaini et al.*, 2005; *Pudasaini and Hutter*, 2007].

4.3. Depth Averaging

[30] For a given function $f = f(t, x, y, z)$, the depth-averaging is denoted by $\bar{f} = \bar{f}(t, x, y)$ and is defined as $\bar{f} = \frac{1}{h}\int_b^s f dz$,

where $h = s - b$ is the debris flow depth (in the direction normal to the substrate surface), $b = b(t, x, y)$ and $s = s(t, x, y)$ are the basal- and the free-surface of the flow. Depth averaging poses great challenges in developing shallow flow equations, particularly for multiphase flows. Following *Savage and Hutter* [1989], I assume that the average of a product is approximated by the product of the averages, i.e., for two given functions f and g,

$$\overline{fg} \approx \overline{f}\,\overline{g}. \tag{25}$$

[31] This is called the 'factorization of the mean'. Then, it follows that the mean of the reciprocal is the reciprocal of the mean:

$$\int_b^s \frac{f}{g}dz = \int_b^s fg^{-1}dz = h\overline{fg^{-1}} = h\overline{f}\,\overline{g^{-1}} = h\overline{f}(\bar{g})^{-1} = h\overline{f}/\bar{g}. \tag{26}$$

This resulted simply from the well excepted classical assumption of the factorization of the mean. This is so because, $1 = \overline{gg^{-1}} = \overline{g}\,\overline{g^{-1}}$ which implies $\overline{g^{-1}} = (\bar{g})^{-1}$. However, these approximations are subject to error [*Iverson and Denlinger*, 2001; *Pitman and Le*, 2005; *Pudasaini et al.*, 2005; *Pudasaini and Hutter*, 2007]. Although (26) is a straightforward and simple consequence of (25) it will have great contributions in depth averaging the expressions associated with the drag force, virtual mass force, quasi Reynolds numbers, etc. This was not realized before.

4.3.1. Basal and Depth Averaged Pressure Terms

[32] From (14f), (17), and (24) (with $\partial p/\partial z = g^z$) the depth-averaged fluid and solid pressures are:

$$\begin{aligned}
&p_{b_f} = -g^z h, \bar{p} = -\frac{1}{2}g^z h = \frac{1}{2}p_{b_f},\\
&\alpha_s T_{zz}|_b = p_{b_s} = (1-\gamma)\alpha_s p_{b_f}, \quad \alpha_s(\mathbf{n}\cdot\mathbf{Tn})|_b = p_{b_s},\\
&\overline{\alpha_s T_{xx}} = -\frac{1}{2}K_x(1-\gamma)\bar{\alpha}_s g^z h, \quad \overline{\alpha_s T_{yy}} = -\frac{1}{2}K_y(1-\gamma)\bar{\alpha}_s g^z h.
\end{aligned} \tag{27}$$

In these equations, p_{b_f} and p_{b_s} are the effective fluid and solid pressures at the basal surface.

4.3.2. Depth Averaged Mass Balance Equations

[33] Adding (14a) and (14b) implies that the mixture is divergence-free, $\nabla\cdot\left(\alpha_s\mathbf{u}_s + \alpha_f\mathbf{u}_f\right) = 0$. Therefore, $\left(\alpha_s\mathbf{u}_s + \alpha_f\mathbf{u}_f\right)$ behaves as the mixture velocity. Applying the Leibniz rule to this equation [see *Pudasaini and Hutter*, 2007] and employing the kinematic boundary conditions for the mixture, one obtains:

$$\begin{aligned}
&\int_b^s \left[\frac{\partial}{\partial x}\left(\alpha_s u_s + \alpha_f u_f\right) + \frac{\partial}{\partial y}\left(\alpha_s v_s + \alpha_f v_f\right) + \frac{\partial}{\partial z}\left(\alpha_s w_s + \alpha_f w_f\right)\right]dz\\
&= \frac{\partial}{\partial x}\left[h\overline{\left(\alpha_s u_s + \alpha_f u_f\right)}\right] + \frac{\partial}{\partial y}\left[h\overline{\left(\alpha_s v_s + \alpha_f v_f\right)}\right]\\
&\quad - \left[\left(\alpha_s u_s + \alpha_f u_f\right)\frac{\partial z}{\partial x} + \left(\alpha_s v_s + \alpha_f v_f\right)\frac{\partial z}{\partial y} - \left(\alpha_s w_s + \alpha_f w_f\right)\right]_b^s\\
&= \frac{\partial}{\partial x}\left[h\left(\overline{\alpha_s u_s} + \overline{\alpha_f u_f}\right)\right] + \frac{\partial}{\partial y}\left[h\left(\overline{\alpha_s v_s} + \overline{\alpha_f v_f}\right)\right] + \frac{\partial h}{\partial t}.
\end{aligned} \tag{28}$$

Assuming that the mean can be factorized the depth-averaged mixture mass balance is obtained

$$\frac{\partial h}{\partial t} + \frac{\partial}{\partial x}\left[h\left(\overline{\alpha_s}\,\overline{u_s} + \overline{\alpha_f}\,\overline{u_f}\right)\right] + \frac{\partial}{\partial y}\left[h\ \left(\overline{\alpha_s}\,\overline{v_s} + \overline{\alpha_f}\,\overline{v_f}\right)\right] = 0. \tag{29}$$

From (14a) and the kinematic boundary conditions, the depth-averaged solid-phase mass balance takes the form

$$\frac{\partial}{\partial t}(h\bar{\alpha}_s) + \frac{\partial}{\partial x}[h\overline{\alpha_s u_s}] + \frac{\partial}{\partial y}[h\overline{\alpha_s v_s}] = 0. \tag{30}$$

Analogously, from (14b), the depth-averaged fluid-phase mass balance yields:

$$\frac{\partial}{\partial t}\left(h\bar{\alpha}_f\right) + \frac{\partial}{\partial x}\left[h\overline{\alpha_f u_f}\right] + \frac{\partial}{\partial y}\left[h\overline{\alpha_f v_f}\right] = 0. \tag{31}$$

4.3.3. Depth Averaged Momentum Balance Equations

[34] *Solid-phase.* To obtain the averaged momentum balance equations for the solid phase, consider the x-direction solid momentum equation (15). By depth-averaging the inertial part of the equation and applying the kinematic boundary conditions together with the Leibniz rule of integration we obtain

$$\begin{aligned}
&\int_b^s (1+\gamma\mathcal{C})\left[\frac{\partial}{\partial t}(\alpha_s u_s) + \frac{\partial}{\partial x}\left(\alpha_s u_s^2\right) + \frac{\partial}{\partial y}(\alpha_s u_s v_s) + \frac{\partial}{\partial z}(\alpha_s u_s w_s)\right]dz\\
&= h\overline{(1+\gamma\mathcal{C})}\,\overline{\left[\frac{\partial}{\partial t}(\alpha_s u_s) + \frac{\partial}{\partial x}\left(\alpha_s u_s^2\right) + \frac{\partial}{\partial y}(\alpha_s u_s v_s) + \frac{\partial}{\partial z}(\alpha_s u_s w_s)\right]}\\
&= \left(1+\gamma\bar{\mathcal{C}}\right)\int_b^s \left[\frac{\partial}{\partial t}(\alpha_s u_s) + \frac{\partial}{\partial x}\left(\alpha_s u_s^2\right) + \frac{\partial}{\partial y}(\alpha_s u_s v_s) + \frac{\partial}{\partial z}(\alpha_s u_s w_s)\right]dz\\
&= \left(1+\gamma\bar{\mathcal{C}}\right)\left\{\left[\frac{\partial}{\partial t}(h\overline{\alpha_s u_s}) + \frac{\partial}{\partial x}\left(h\overline{\alpha_s u_s^2}\right) + \frac{\partial}{\partial y}(h\overline{\alpha_s u_s v_s})\right]\right.\\
&\quad \left. - \left[\alpha_s u_s\left(\frac{\partial z}{\partial t} + u_s\frac{\partial z}{\partial x} + v_s\frac{\partial z}{\partial y} - w_s\right)\right]_b^s\right\}\\
&= \left(1+\gamma\bar{\mathcal{C}}\right)\left[\frac{\partial}{\partial t}(h\overline{\alpha_s u_s}) + \frac{\partial}{\partial x}\left(h\overline{\alpha_s u_s^2}\right) + \frac{\partial}{\partial y}(h\overline{\alpha_s u_s v_s})\right],
\end{aligned} \tag{32}$$

where $\bar{\mathcal{C}}(\alpha_s) = \mathcal{C}(\bar{\alpha}_s)$. In (32) factorization of the mean is applied repeatedly. Here, it is shown for the factor $(1+\gamma\mathcal{C})$:

$$\begin{aligned}
\overline{(1+\gamma\mathcal{C})} &= 1 + \gamma\bar{\mathcal{C}} = 1 + \frac{1}{2}\gamma\overline{\left(\frac{1+2\alpha_s}{\alpha_f}\right)} = 1 + \frac{1}{2}\gamma\left(\frac{1+2\overline{\alpha_s}}{\overline{\alpha_f}}\right)\\
&= 1 + \frac{1}{2}\gamma\left[\frac{1+2\overline{\alpha_s}}{(1-\overline{\alpha_s})}\right] = 1 + \gamma\mathcal{C}(\overline{\alpha_s}).
\end{aligned} \tag{33}$$

[35] Now, consider the solid stress terms and apply the dynamic boundary conditions to obtain:

$$\begin{aligned}
&-\int_b^s \left\{\varepsilon\frac{\partial}{\partial x}(\alpha_s T_{xx}) + \varepsilon\mu\frac{\partial}{\partial y}\left(\alpha_s T_{xy}\right) + \mu\frac{\partial}{\partial z}(\alpha_s T_{xz})\right\}dz\\
&= -\varepsilon\frac{\partial}{\partial x}\left[h\left(\overline{\alpha_s T_{xx}}\right)\right] - \varepsilon\mu\frac{\partial}{\partial y}\left[h\left(\overline{\alpha_s T_{xy}}\right)\right]\\
&\quad + \left[\varepsilon\alpha_s T_{xx}\frac{\partial z}{\partial x} + \varepsilon\mu\alpha_s T_{xy}\frac{\partial z}{\partial y} - \mu\alpha_s T_{xz}\right]_b^s\\
&= -\left\{\varepsilon\frac{\partial}{\partial x}\left[h\left(\overline{\alpha_s T_{xx}}\right)\right] + \varepsilon\mu\frac{\partial}{\partial y}\left[h\left(\overline{\alpha_s T_{xy}}\right)\right] + \alpha_s(\mathbf{n}\cdot\mathbf{Tn})|_b\right.\\
&\quad \left.\cdot\left(\frac{u_s}{|\mathbf{u}_s|}\tan\delta + \varepsilon\frac{\partial b}{\partial x}\right)\right\}.
\end{aligned} \tag{34}$$

Following *Savage and Hutter* [1989], *Gray et al.* [1999], and *Pudasaini and Hutter* [2007] the shear stress T_{xy} is negligible because $\varepsilon\mu$ is of $O(\varepsilon^{1+\nu})$, $0 < \nu < 1$. This is a consequence of the Coulomb rheology. This term, however, was retained in *Iverson and Denlinger* [2001] and *Pitman and Le* [2005]. Depth averaging of the term $\varepsilon\gamma p\partial\alpha_s/\partial x$ in (15) associated with the buoyancy force, with the remark at the end of section 4.1, becomes:

$$-\varepsilon\gamma\int_b^s \alpha_s\frac{\partial p}{\partial x}dz = \varepsilon\gamma\int_b^s \alpha_s\frac{\partial}{\partial x}[g^z(s-z)]dz = \varepsilon\gamma\bar{\alpha}_s g^z h\left[\frac{\partial h}{\partial x}+\frac{\partial b}{\partial x}\right] = \varepsilon\gamma\bar{\alpha}_s\left[\frac{\partial}{\partial x}\left(g^z h^2/2\right)+g^z h\frac{\partial b}{\partial x}\right]. \tag{35}$$

[36] By applying the shallow-flow assumption to approximate the velocities by their means, depth-averaged expression for drag (last term in the right-hand side of (15)) yields:

$$\int_b^s \frac{\alpha_s\alpha_f(1-\gamma)}{\left[\varepsilon\ \mathcal{U}_T\left\{\mathcal{P}\mathcal{F}(Re_p)+(1-\mathcal{P})\mathcal{G}(Re_p)\right\}\right]^J}\left(u_f-u_s\right)|\mathbf{u}_f-\mathbf{u}_s|^{J-1}dz = \frac{\bar{\alpha}_s\bar{\alpha}_f(1-\gamma)}{\left[\varepsilon\mathcal{U}_T\left\{\mathcal{P}\bar{\mathcal{F}}(Re_p)+(1-\mathcal{P})\bar{\mathcal{G}}(Re_p)\right\}\right]^J}\left(\bar{u}_f-\bar{u}_s\right)\left|\bar{\mathbf{u}}_f-\bar{\mathbf{u}}_s\right|^{J-1}h, \tag{36}$$

where $\bar{\mathcal{F}}(\alpha_s,\alpha_f)=\mathcal{F}(\bar{\alpha}_s,\bar{\alpha}_f)$ and $\bar{\mathcal{G}}(\alpha_f)=\mathcal{G}(\bar{\alpha}_f)$. In general, $\mathcal{P}$ can be written as $\mathcal{P}=\mathcal{P}(\bar{\alpha}_s,\nabla\bar{\alpha}_s)$. The gravity term $(\alpha_s g^x)$ in (15) is depth-averaged, which simply becomes $\bar{\alpha}_s g^x h$. Combining equations (32), (34)–(36) and $\bar{\alpha}_s g^x h$ constitutes the x-component of the depth-averaged solid momentum equation. An analogous expression is derived for the y-component of the depth-averaged solid momentum equation.

[37] *Fluid-phase.* Depth averaging of the fluid momentum equations is more involved and poses substantial difficulties compared to averaging of the solid momentum equations, owing to the viscous forces, the enhanced fluid-stress tensor, and the depth distribution of the solid volume fraction. Here, the expression for the depth-averaged x-direction fluid momentum equation is derived. The inertial, gravity, and the drag terms can be depth-averaged exactly as for the solid-phase depth-averaged equation. Following *Pudasaini et al.* [2005], the pressure and Newtonian viscous terms associated with N_R are depth-averaged to yield:

$$\varepsilon\left\{-\bar{\alpha}_f\left[\frac{\partial}{\partial x}(h\bar{p})+p_{b_f}\frac{\partial b}{\partial x}\right]+\frac{h}{N_R}\left[2\frac{\partial^2\bar{u}_f}{\partial x^2}+\frac{\partial^2\bar{v}_f}{\partial y\partial x}+\frac{\partial^2\bar{u}_f}{\partial y^2}-\frac{\chi\bar{u}_f}{\varepsilon^2h^2}\right]\right\}+O\left(\varepsilon^{1+\nu}\right), \tag{37}$$

where χ is a shape factor (e.g., parabolic-type) that includes vertical shearing of fluid velocity (χ = 3 in *Iverson and Denlinger* [2001] and *Pudasaini et al.* [2005]). For strictly shallow flows $\chi \equiv 0$ because depth-variation of u_f and v_f are neglected. Depth-averaging the non-Newtonian viscous term reduces the 6th term on the right-hand side of (18) to:

$$\begin{aligned}\frac{2\varepsilon}{N_{R_A}}\int_b^s\frac{\partial}{\partial x}\left(\frac{\partial\alpha_s}{\partial x}\left(u_f-u_s\right)\right)dz &= \frac{2\varepsilon}{N_{R_A}}\left\{\frac{\partial}{\partial x}\left(h\ \overline{\frac{\partial\alpha_s}{\partial x}\left(u_f-u_s\right)}\right)-\left[\frac{\partial\alpha_s}{\partial x}\left(u_f-u_s\right)\frac{\partial z}{\partial x}\right]_b^s\right\}\\ &= \frac{2\varepsilon}{N_{R_A}}\left[\frac{\partial}{\partial x}\left(h\ \frac{\partial\bar{\alpha}_s}{\partial x}\left(\bar{u}_f-\bar{u}_s\right)\right)-\frac{\partial\bar{\alpha}_s}{\partial x}\left(\bar{u}_f-\bar{u}_s\right)\frac{\partial h}{\partial x}\right]\\ &= \frac{2\varepsilon}{N_{R_A}}\left[h\frac{\partial}{\partial x}\left(\frac{\partial\bar{\alpha}_s}{\partial x}\left(\bar{u}_f-\bar{u}_s\right)\right)\right].\end{aligned} \tag{38}$$

[38] As in the derivation of (37), I assume that $\partial\alpha_s/\partial x|_s$ and $\overline{\partial\alpha_s/\partial x}|_b$ are approximated by $\partial\bar{\alpha}_s/\partial x$ and that $\overline{\partial\alpha_s/\partial x}\approx\partial\bar{\alpha}_s/\partial x$. From the shallow water hypothesis, the basal and free surface velocity components (u_s, v_s) and (u_f, v_f) are approximated by their means. Hence, the 7th term on the right-hand side of (18) becomes:

$$\frac{\varepsilon}{N_{R_A}}\int_b^s\frac{\partial}{\partial y}\left(\frac{\partial\alpha_s}{\partial x}\left(v_f-v_s\right)+\frac{\partial\alpha_s}{\partial y}\left(u_f-u_s\right)\right)dz = \frac{\varepsilon}{N_{R_A}}\left[h\left\{\frac{\partial}{\partial y}\left(\frac{\partial\bar{\alpha}_s}{\partial x}\left(\bar{v}_f-\bar{v}_s\right)+\frac{\partial\bar{\alpha}_s}{\partial y}\left(\bar{u}_f-\bar{u}_s\right)\right)\right\}\right]. \tag{39}$$

Because I assume that the expression associated with w is negligible, the 8th term on the right-hand side of (18) becomes

$$\frac{\varepsilon}{\varepsilon^2N_{R_A}}\int_b^s\frac{\partial}{\partial z}\left(\frac{\partial\alpha_s}{\partial z}\left(u_f-u_s\right)\right)dz = \frac{\varepsilon}{\varepsilon^2N_{R_A}}\left[\frac{\partial\alpha_s}{\partial z}\left(u_f-u_s\right)\right]_b^s = \frac{\varepsilon}{\varepsilon^2N_{R_A}}\left(\bar{u}_f-\bar{u}_s\right)\left[\frac{\partial\alpha_s}{\partial z}\right]_b^s = -\frac{\varepsilon h}{N_{R_A}}\left[\frac{\xi\left(\bar{u}_f-\bar{u}_s\right)\bar{\alpha}_s}{\varepsilon^2h^2}\right]. \tag{40}$$

In (40) the shape factor ξ takes into account different distributions of solids volume fraction, α_s, (parabolic or linear) with depth. For a uniform distribution of α_s with depth, $\xi \equiv 0$. The negative sign indicates that the concentration gradient decreases with increasing depth direction, as has been observed [see *Takahashi*, 2007]. Collecting (38)–(40), one obtains the depth-averaged solid-volume-fraction-gradient induced non-Newtonian viscous contribution. Combining (37)–(40) and expressions similar to (32) and (36) for inertial and drag terms, and gravity ($\bar{\alpha}_f g^x h$) yields the depth-averaged x-direction fluid momentum equation. The depth-averaged y-direction fluid momentum equation can be derived analogously. In the following equations, the over bars are dropped for brevity.

5. The Model Equations

[39] The depth-averaged model equations are written in standard and well structured conservative form. The mass balance equations for the mixture as a whole, and for the solid and fluid phases are, respectively:

$$\frac{\partial h}{\partial t}+\frac{\partial}{\partial x}\left[h\left(\alpha_s u_s+\alpha_f u_f\right)\right]+\frac{\partial}{\partial y}\left[h\left(\alpha_s v_s+\alpha_f v_f\right)\right]=0, \tag{41a}$$

$$\frac{\partial}{\partial t}\left(\alpha_s h\right)+\frac{\partial}{\partial x}\left(\alpha_s h u_s\right)+\frac{\partial}{\partial y}\left(\alpha_s h v_s\right)=0, \tag{41b}$$

$$\frac{\partial}{\partial t}\left(\alpha_f h\right)+\frac{\partial}{\partial x}\left(\alpha_f h u_f\right)+\frac{\partial}{\partial y}\left(\alpha_f h v_f\right)=0. \tag{41c}$$

Similarly, collecting the terms from (27) and (32)–(36) and (37)–(40) yields the depth-averaged momentum conservation equations for the solid and the fluid phases,

$$\frac{\partial}{\partial t}\left[\alpha_s h\left(u_s-\gamma\mathcal{C}\left(u_f-u_s\right)\right)\right]+\frac{\partial}{\partial x}\left[\alpha_s h\left(u_s^2-\gamma\mathcal{C}\left(u_f^2-u_s^2\right)+\beta_x\frac{h}{2}\right)\right]+\frac{\partial}{\partial y}\left[\alpha_s h\left(u_s v_s-\gamma\mathcal{C}\left(u_f v_f-u_s v_s\right)\right)\right]=h\mathcal{S}_{x_s}, \quad (42a)$$

$$\frac{\partial}{\partial t}\left[\alpha_s h\left(v_s-\gamma\mathcal{C}\left(v_f-v_s\right)\right)\right]+\frac{\partial}{\partial x}\left[\alpha_s h\left(u_s v_s-\gamma\mathcal{C}\left(u_f v_f-u_s v_s\right)\right)\right]+\frac{\partial}{\partial y}\left[\alpha_s h\left(v_s^2-\gamma\mathcal{C}\left(v_f^2-v_s^2\right)+\beta_y\frac{h}{2}\right)\right]=h\mathcal{S}_{y_s}, \quad (42b)$$

$$\frac{\partial}{\partial t}\left[\alpha_f h\left(u_f+\frac{\alpha_s}{\alpha_f}\mathcal{C}\left(u_f-u_s\right)\right)\right]+\frac{\partial}{\partial x}\left[\alpha_f h\left(u_f^2+\frac{\alpha_s}{\alpha_f}\mathcal{C}\left(u_f^2-u_s^2\right)\right)\right]+\frac{\partial}{\partial y}\left[\alpha_f h\left(u_f v_f+\frac{\alpha_s}{\alpha_f}\mathcal{C}\left(u_f v_f-u_s v_s\right)\right)\right]=h\mathcal{S}_{x_f}, \quad (42c)$$

$$\frac{\partial}{\partial t}\left[\alpha_f h\left(v_f+\frac{\alpha_s}{\alpha_f}\mathcal{C}\left(v_f-v_s\right)\right)\right]+\frac{\partial}{\partial x}\left[\alpha_f h\left(u_f v_f+\frac{\alpha_s}{\alpha_f}\mathcal{C}\left(u_f v_f-u_s v_s\right)\right)\right]+\frac{\partial}{\partial y}\left[\alpha_f h\left(v_f^2+\frac{\alpha_s}{\alpha_f}\mathcal{C}\left(v_f^2-v_s^2\right)\right)\right]=h\mathcal{S}_{y_f}, \quad (42d)$$

in which $\beta_x = \varepsilon K_x p_{b_s}$, $\beta_y = \varepsilon K_y p_{b_s}$, $p_{b_f} = -g^z$, $p_{b_s} = (1-\gamma)\,p_{b_f}$. Here, p_{b_f} and p_{b_s} are the effective fluid and solid pressures at the base. In (42), the source terms are

$$\mathcal{S}_{x_s}=\alpha_s\left[g^x-\frac{u_s}{|\mathbf{u}_s|}\tan\delta p_{b_s}-\varepsilon p_{b_s}\frac{\partial b}{\partial x}\right]-\varepsilon\alpha_s\gamma p_{b_f}\left[\frac{\partial h}{\partial x}+\frac{\partial b}{\partial x}\right]+C_{DG}\left(u_f-u_s\right)\left|\mathbf{u}_f-\mathbf{u}_s\right|^{\jmath-1}, \quad (43)$$

$$\mathcal{S}_{y_s}=\alpha_s\left[g^y-\frac{v_s}{|\mathbf{u}_s|}\tan\delta p_{b_s}-\varepsilon p_{b_s}\frac{\partial b}{\partial y}\right]-\varepsilon\alpha_s\gamma p_{b_f}\left[\frac{\partial h}{\partial y}+\frac{\partial b}{\partial y}\right]+C_{DG}\left(v_f-v_s\right)\left|\mathbf{u}_f-\mathbf{u}_s\right|^{\jmath-1}, \quad (44)$$

$$\mathcal{S}_{x_f}=\alpha_f\left[g^x-\varepsilon\left[\frac{1}{h}\frac{\partial}{\partial x}\left(\frac{h^2}{2}p_{b_f}\right)+p_{b_f}\frac{\partial b}{\partial x}-\frac{1}{\alpha_f N_R}\cdot\left\{2\frac{\partial^2 u_f}{\partial x^2}+\frac{\partial^2 v_f}{\partial y\partial x}+\frac{\partial^2 u_f}{\partial y^2}-\frac{\chi u_f}{\varepsilon^2 h^2}\right\}+\frac{1}{\alpha_f N_{R_A}}\cdot\left\{2\frac{\partial}{\partial x}\left(\frac{\partial\alpha_s}{\partial x}\left(u_f-u_s\right)\right)+\frac{\partial}{\partial y}\left(\frac{\partial\alpha_s}{\partial x}\left(v_f-v_s\right)+\frac{\partial\alpha_s}{\partial y}\left(u_f-u_s\right)\right)\right\}-\frac{\xi\alpha_s\left(u_f-u_s\right)}{\varepsilon^2\alpha_f N_{R_A}h^2}\right]\right]-\frac{1}{\gamma}C_{DG}\left(u_f-u_s\right)\left|\mathbf{u}_f-\mathbf{u}_s\right|^{\jmath-1}, \quad (45)$$

$$\mathcal{S}_{y_f}=\alpha_f\left[g^y-\varepsilon\left[\frac{1}{h}\frac{\partial}{\partial y}\left(\frac{h^2}{2}p_{b_f}\right)+p_{b_f}\frac{\partial b}{\partial y}-\frac{1}{\alpha_f N_R}\left\{2\frac{\partial^2 v_f}{\partial y^2}+\frac{\partial^2 u_f}{\partial x\partial y}+\frac{\partial^2 v_f}{\partial x^2}-\frac{\chi v_f}{\varepsilon^2 h^2}\right\}+\frac{1}{\alpha_f N_{R_A}}\cdot\left\{2\frac{\partial}{\partial y}\left(\frac{\partial\alpha_s}{\partial y}\left(v_f-v_s\right)\right)+\frac{\partial}{\partial x}\left(\frac{\partial\alpha_s}{\partial y}\left(u_f-u_s\right)+\frac{\partial\alpha_s}{\partial x}\left(v_f-v_s\right)\right)\right\}-\frac{\xi\alpha_s\left(v_f-v_s\right)}{\varepsilon^2\alpha_f N_{R_A}h^2}\right]\right]-\frac{1}{\gamma}C_{DG}\left(v_f-v_s\right)\left|\mathbf{u}_f-\mathbf{u}_s\right|^{\jmath-1}, \quad (46)$$

where,

$$C_{DG}=\frac{\alpha_s\alpha_f(1-\gamma)}{\left[\varepsilon\mathcal{U}_T\left\{\mathcal{P}\mathcal{F}\left(Re_p\right)+(1-\mathcal{P})\mathcal{G}\left(Re_p\right)\right\}\right]^{\jmath}},$$
$$\mathcal{F}=\frac{\gamma}{180}\left(\frac{\alpha_f}{\alpha_s}\right)^3 Re_p,\qquad \mathcal{G}=\alpha_f^{M\left(Re_p\right)-1},$$
$$\gamma=\frac{\rho_f}{\rho_s},\ \mathcal{C}=\frac{1}{2}\left(\frac{1+2\alpha_s}{\alpha_f}\right),\quad Re_p=\frac{\rho_f d\mathcal{U}_T}{\eta_f},$$
$$N_R=\frac{\sqrt{gL}H\rho_f}{\alpha_f\eta_f},\quad N_{R_A}=\frac{\sqrt{gL}H\rho_f}{\mathcal{A}\eta_f}. \quad (47)$$

Simple linear (laminar-type, at low velocity) or quadratic (turbulent-type, at high velocity) drag is associated with $\jmath = 1$ or 2, respectively. The virtual mass effect ($\mathcal{C}$) is present in all inertial terms (terms on the left hand side of (42)). For simplicity, $\mathcal{C}$ is assumed to be a constant; hence $\mathcal{C} = 0.5$ is applied. Given the material parameters listed in (47) and the basal topography, $b = b(x, y)$, equations (41)–(46) allow the debris flow depth h, volume fraction of the fluid α_f, and the depth-averaged velocity components for solid u_s and v_s and for fluid u_f and v_f parallel to the basal surface to be computed as functions of space and time, once appropriate initial and (numerical) boundary conditions are prescribed.

6. Discussion on the Important Features of the New Model Equations

[40] The final model equations (41)–(46) are written as well structured hyperbolic-parabolic partial differential equations in conservative form. There are several important features of the new model equations. Here, the most important physical aspects and their consequences and applicability are discussed. These model equations are also compared with other existing model equations in the literature (Appendix C).

6.1. Inertial Terms

[41] There are four important aspects in the inertial and pressure terms shown in (42). (*i*) The terms associated with β in the solid momentum equations (42a)–(42b) account for the buoyancy-reduced lateral pressures. The solid load is reduced by the buoyancy force as modeled by the factor $(1-\gamma)$. As the density ratio between solid and fluid approaches unity, the solid normal load vanishes, and hence, the hydraulic pressure gradient due to solids disappears. In this limiting case, the flow is neutrally buoyant [*Bagnold*, 1954] and the left-hand sides of (42a)–(42b) are purely inertial. (*ii*) Only the solid momentum equations (42a)–(42b) include the density ratio γ. (*iii*) The presence of the virtual mass terms (through $\mathcal{C}$) is remarkable. It provides a strong coupling between the solid (u_s, v_s) and fluid (u_f, v_f) velocity components. The coupling occurs not only between the stream-wise (u_s and u_f) and cross-stream velocity components (v_s and v_f) but there are cross couplings between (u_s, v_s) and (u_f, v_f). However, if the relative acceleration of the solids with respect to the fluid is negligible, then all terms associated with $\mathcal{C}$ vanish (Appendix C1). Thus, the velocity coupling induced in the streamwise and cross-streamwise directions by the virtual mass is an important feature of the new model equations. Even if all source terms are neglected (i.e., $\mathcal{S}_x = 0$, $\mathcal{S}_y = 0$), velocity coupling

remains effective through the virtual mass terms. The solid volume fraction (α_s) always appears as a multiple of $\mathcal{C}$. (*iv*) If the solid and fluid components are interlocked (that is, the relative velocity between phases is negligible) then all the terms due to virtual mass vanish, and equations (42) reduce to two equations, representing the stream-wise, and cross-stream bulk momentum (Appendices C1 and C2).

6.2. Source Terms

[42] The source terms for the solid momentum equations (43)–(44) have multiple contributions to force: (1) gravity, Coulomb friction and the topographic slope gradients. These terms (the first square bracket) appear in model for single-phase (granular) and mixture flows even if $\gamma = 0$ (i.e., the fluid contribution is neglected). If a flow is neutrally buoyant (this can happen in highly viscous natural debris flows [see, e.g., *McArdell et al.*, 2007]), the contributions due to Coulomb friction, and the basal-surface gradient vanish because the basal surface does not experience any solid load, and the solid shear stress vanishes. Under these conditions of hydrodynamic support of the particles by the fluid, the debris mass is fully fluidized (or lubricated) and moves very economically promoting long travel distances. (2) The terms associated with the second square brackets are due to the buoyancy force that include free-surface and basal-surface gradients. (3) The generalized drag terms (C_{DG}) associated with uniform flows are described by the last terms, and play an important role in the dynamics of two-phase debris flows as they strongly couple stream-wise solid and fluid velocities. These drag coefficients explicitly incorporate many essential physical parameters. The generalized drag is modeled by a linear combination of $\mathcal{F}$ and $\mathcal{G}$. The behavior depends on the interpolation parameter $\mathcal{P}$ between the contribution of fluid flow through a densely packed solid $(\mathcal{F})$ (Kozeny-Carman packing) and the contribution of particles moving through a fluid $(\mathcal{G})$. For values of $\mathcal{P}$ greater than zero, the generalized drag achieves minimum values (for α_s close to zero), and increases as α_s increases. Large values of $\mathcal{P}$ correspond to fluid flow through the solid, which induces more drag in the flow. Therefore, C_{DG} serves as a generalized drag coefficient for two-phase, viscous debris flows and dispersive, particle-laden flows, and offers ability to simulate a wide spectrum of geophysical mass flows (including flows of lahar, mudflow, mud-flood and hyper-concentrated flows). In four special situations, C_{DG} vanishes: when the relative velocity between solids and fluid is negligible, when the flow is neutrally buoyant or when either solid (pure fluid flow) or fluid volume fraction vanishes (dry grain flow).

[43] The source terms for the fluid-momentum equations (45)–(46) also have multiple contributions to force. The first three terms in (45) emerge from the gravity load applied to the fluid phase (first term), the fluid pressure at the bed (second term) and the topographic slope (third term). The fourth group of terms associated with N_R emerges from the viscous force contribution of the fluid phase. The fifth group of terms associated with N_{R_A} occurs because, viscous shear stress is enhanced by the solid-volume-fraction gradient. These are non-Newtonian viscous contributions. When gradients of the solid volume fraction, and/or the relative motions between the solid and fluid phases are not negligible, these terms play important role. In typical situations, the terms associated with N_R may be neglected, e.g., when N_R is sufficiently larger than the velocity diffusion contributions (terms associated with N_R). Even when terms with N_R are negligible, terms associated with N_{R_A} may still be important, because they depend on the complex structure of the terms associated with N_{R_A}. In fact, it depends on the second gradients of the solid volume fraction, and the first gradients of the relative motions between the phases. In many flow situations, these gradients can be large enough to control the effect of the factor $1/N_{R_A}$. For example, when a natural-dam failure or landslide-induced debris flow begins, mixing between solid and fluid phases starts. In this situation, the diffusion coefficient (see, section 6.5) associated with N_{R_A} can become very large. When bank failure delivers solid material to a relatively low-solid-concentration stream, the solid volume fraction gradient and the relative motion between the solid and the fluid is large. Another typical situation is a submarine debris release or subaerial debris plunging into a river, or a mountain lake or a hydropower dam [see, e.g., *Crosta et al.*, 2004; *Strom and Korup*, 2006]. In these complex flows, concentration gradients of solids change rapidly. Furthermore, the second gradient of α_s and its product with the relative velocity can be even larger. Yet, in another situation, when topographic gradients change rapidly, concentration gradients of the solid can develop or diffuse depending on positive or negative curvatures of topography. This means that depending on the flow situation, and boundary conditions, the terms associated with N_{R_A} may play a significant role in the debris flow dynamics. Existing debris-flow and particle-laden geophysical mass flow models do not include these effects. The last terms in (45) and (46) are due to the drag force induced by the relative velocities between the solid and fluid phases.

6.3. Viscous Terms

[44] In situations when grains are dispersed in a fluid and the grain-grain friction is negligible, the earth pressure coefficient $K = 1$ (effectively $\delta \equiv 0$, $\phi = 0$, $\mathcal{F} \equiv 0$), and inclusion of the viscous stresses is important because the grain shear stress terms $-\alpha_s(u_s/|\mathbf{u}|_s)\tan\delta p_{b_s}$, $-\alpha_s(v_s/|\mathbf{u}|_s)\tan\delta p_{b_s}$ can be neglected. This leads to gravity-driven buoyant grain flows that are resisted by viscous and drag forces, and the relative acceleration between solid and fluid components (virtual mass). Due to buoyancy, the basal solid stress, p_{b_s} is written in terms of the fluid pressure, p_{b_f}. For neutrally buoyant particles, the density ratio $\gamma = 1$, and basal solid weight (p_{b_s}) vanishes. Consequently, Coulomb friction disappears, lateral solid pressure gradients vanish (because $\beta = 0$), the drag coefficient is zero, $C_{DG} = 0$, and that the basal slope effect on the solid phase also vanishes. The only remaining solid forces ($\alpha_s g^x$ in (43) and $\alpha_s g^y$ in (44)) are due to gravity, and the force associated with buoyancy (the second square brackets in (43) and 44)). However, for the fluid phase, the viscous and gravity forces are effective in addition to the force induced by the gradient of the solid volume fraction ($\nabla\alpha_s$), the fluid pressure gradient at the base, and the fluid pressure exerted on the topography (see, (45) and (46)). In this situation, the importance of α_s as a field variable becomes clear. The appearance of ε in (45) and (46) indicates the following. The fluid viscous terms, associated with both N_R and N_{R_A}, are as important as the basal (slope) gradient terms ($\varepsilon\alpha_s p_{b_s}\partial b/\partial x$) and ($\varepsilon\alpha_s p_{b_s}\partial b/\partial y$), the pressure gradient

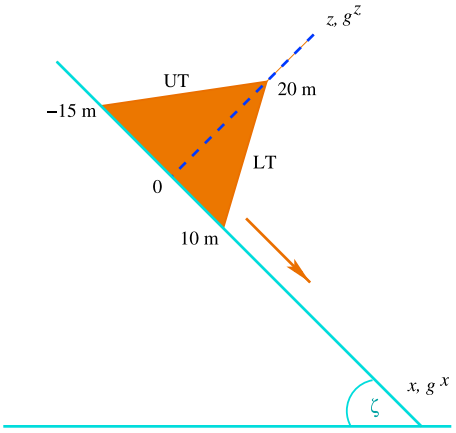

Figure 1. Geometry and initial setting for the two-phase debris flow simulation. Initially, the upper triangle (UT) and the lower triangle (LT) are filled with uniform mixture of solid and fluid either equal or with different initial solid volume fraction (α_s). The channel is inclined at an angle $\zeta = 45°$. Physical parameters are explained in the beginning of section 7.

terms $\partial(\alpha_s\beta_x h^2/2)/\partial x$ and $\partial(\alpha_s\beta_y h^2/2)/\partial y$ in solid momentum equations (42a)–(42b), (43), and (44), and $\varepsilon\alpha_f\partial(p_{b_f}h^2/2)/\partial x$, $\varepsilon\alpha_f\partial(p_{b_f}h^2/2)/\partial y$ in the fluid momentum equations (42c)–(42d), (45), and (46). The importance of these terms have long been recognized [*Savage and Hutter*, 1989; *Pudasaini and Hutter*, 2003, 2007; *Pitman and Le*, 2005]. Therefore, the viscous terms must also be included in the fluid momentum equations. Since the viscosity η_f is in the denominator of N_R and N_{R_A}, the influence of the terms associated with ε in the fluid momentum equations increases as the magnitude of $u_f - u_s$ increases.

6.4. Drag Coefficients

[45] The appearance of $\varepsilon^{\jmath}$ in the denominator of the drag force coefficient indicates that the drag terms can be of utmost importance as compared to other force terms. Here, ε appeared this way, because the derivation of C_{DG} was based on the vertical terminal velocity [*Richardson and Zaki*, 1954; *Pitman and Le*, 2005]. In shallow flows, bed parallel velocities are typically much higher than vertical velocities. This suggests that the vertical velocity, and thus $\mathcal{U}_T$, is scaled with $\varepsilon\sqrt{gL}$. This automatically produces the factor $1/\varepsilon^{\jmath}$ in the bed parallel drag coefficients (47) and factor $1/\varepsilon^{\jmath-1}$ in the vertical drag coefficients in (17) and (20). Importantly, this introduced drag effects in the fluid pressure and the pressure deviates from hydrostatic in (21). However, in *Pitman and Le* [2005], ε appears only in the numerator of the z component of drag. This is so because they scale $\mathcal{U}_T$ with a surface-parallel velocity scaling.

6.5. Diffusion of Solid Volume Fraction

[46] From (45), the expression associated with N_{R_A} (except $\xi\alpha_s(u_f - u_s)/\varepsilon^2\alpha_f N_{R_A}h^2$) can be written as:

$$h\left[\frac{\partial}{\partial x}\left\{\frac{2}{N_{R_A}}(u_f-u_s)\frac{\partial\alpha_s}{\partial x}\right\}+\frac{\partial}{\partial y}\left\{\frac{1}{N_{R_A}}(v_f-v_s)\frac{\partial\alpha_s}{\partial x}\right\}+\frac{\partial}{\partial y}\left\{\frac{1}{N_{R_A}}(u_f-u_s)\frac{\partial\alpha_s}{\partial y}\right\}\right], \tag{48}$$

where the terms of the form $(u_f - u_s)/N_{R_A}$ play the role of a velocity-dependent dynamic diffusion coefficient for the solid volume fraction α_s. This means that the intensity of diffusion of α_s depends on the magnitude of the relative velocity of solid with respect to the fluid. If $u_f - u_s = 0$ and $v_f - v_s = 0$ there is no diffusion of α_s. Previous models did not consider evolving solid concentration as presented here. However, based on a "definition of the depth-averaged granular dilation rate" for a bulk debris mixture, *George and Iverson* [2011] introduced a simple evolution equation for depth-averaged conservation of granular phase as a linear function of the dilation-rate and the depth-averaged solid volume fraction, but inversely proportional to the debris flow depth. Also note that the diffusion of α_s is inversely proportional to N_{R_A}. Furthermore, the advection of α_s is included in the inertial terms in (42) as a field variable, and α_s also appears in the mass balance equations (41). As in *Pudasaini et al.* [2005], expressions similar to (48) can be written for the terms associated with N_R in (45)–(46). However, here I do not consider changes in α_s owing to erosion or deposition.

7. Simulations of Two-Phase Debris Flows in an Inclined Channel

[47] The conservative structure of the model equations (41)–(42) facilitates numerical integration even when shocks are formed in the field variables [*Pudasaini et al.*, 2005; *Pudasaini and Kröner*, 2008]. Model equations are applied for channel flows and are solved in conservative variables $\mathbf{W} = (h_s, h_f, m_s, m_f)^t$, where $h_s = \alpha_s h$ and $h_f = \alpha_f h$ are the solid and the fluid contributions to the flow heights, and $m_s = \alpha_s h u_s$, $m_f = \alpha_f h u_f$ are the solid and fluid momentum fluxes, respectively. High-resolution, shock-capturing Total Variation Diminishing Non-Oscillatory Central (TVD-NOC) scheme is implemented to solve the model equations numerically [*Nessyahu and Tadmor*, 1990; *Tai et al.*, 2002; *Pudasaini et al.*, 2005; *Pudasaini and Hutter*, 2007; *Pudasaini and Domnik*, 2009] (Appendix D).

[48] *Simulation set-up and focus.* Model equations are integrated for a simple flow configuration in which a debris flow is released from a triangular dam and moves down an inclined one-dimensional channel (slope angle $\zeta = 45°$, Figure 1). The initial triangular mass is divided into two parts: an upper triangle (UT), and a lower triangle (LT), which have either the same or different solid volume fraction. The idea of using different initial solid volume fractions in the front and the back of the debris body is motivated by field observations that the phases can be spatially non-uniformly distributed (see, e.g., *Sano* [2011]). Initially, some parts of the mixture material may be fully saturated, whereas the other parts may be partially saturated. In addition, the material within each triangular zone is uniformly mixed. Internal and basal friction angles of the solid-phase are $\phi = 35°$ and $\delta = 15°$, respectively. Other parameter values are: $\rho_f = 1$, 100 kgm^{-3}, $\rho_s = 2$, 500 kgm^{-3}, $N_R = 150,000$, $N_{R_A} = 30$, $\mathrm{Re}_p = 1$, $\mathcal{U}_T = 1, \mathcal{P} = 0.5, \jmath = 1, \chi = 3, \xi = 5$, respectively. The values chosen for Re_p, $\mathcal{U}_T, \mathcal{P}, \jmath$ are assumed to be typical for laminar debris flows, whereas other parameter values are similar to those measured in the field or used in literature, including *Takahashi* [1991, 2007],

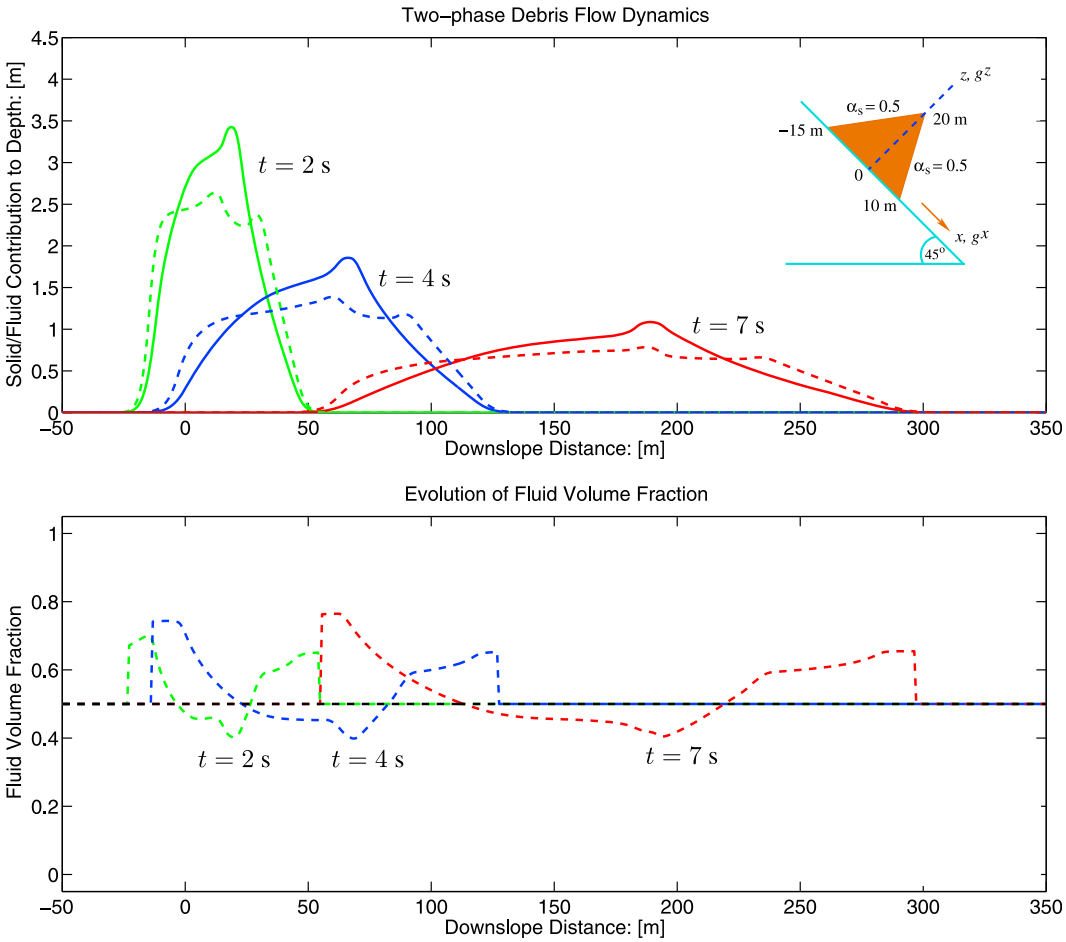

Figure 2. Spatial and temporal evolution of a two-phase debris flow as the mixture moves down an inclined channel as shown in the inset for $t = 0$. Initially, the upper and lower triangles are homogeneously and uniformly filled (50% solid, 50% fluid). (top) The evolution of the solid and the fluid phases, represented by the solid and the dashed lines, respectively. After debris collapse, the fluid rapidly moves in the front- and slowly in the back-ward directions leading to bulging of the fluid in both sides of the debris. It is observed that the front and tail are dominated by the fluid component. (bottom) The non-linear evolution of fluid volume fraction during the debris motion.

Iverson and Denlinger [2001], *Pudasaini et al.* [2005], and *George and Iverson* [2011]. Below, I investigate the spatial and temporal evolution of the solid (solid lines) and fluid (dashed lines) phases, and the fluid volume fraction as the two-phase debris flow moves down the slope. The influence of the initial solid-volume fraction on flow evolution is analyzed. The emphasis of the simulations is to analyze the overall dynamics of the two-phase debris-flow in detail with respect to the influence of the generalized drag, buoyancy, virtual mass, Newtonian viscous stress, and enhanced non-Newtonian viscous stress.

7.1. Evolution of Solid and Fluid Phases, and Influence of Initial Volume Fraction

[49] Simulation results reveal strong influence of the initial distribution of solid volume fraction in the evolution of solid and fluid phases, and the debris dynamics as a whole. Initially, the upper and lower triangles are homogeneously and uniformly filled (50% solid, 50% fluid; Figure 2). After debris collapse the fluid rapidly spreads to both the leading and trailing edges of the debris. As a result, both the leading and trailing edges of the debris flow are dominated by fluid, whereas the central part is dominated by solids. With time, both phases are continuously elongated, and the flow shape changes. This occurs because the entire mass was initially uniformly mixed, and as soon as the mass collapses, the fluid can slide easily and faster in the downslope direction than can the solid grains. This results from the higher frontal resistance for the solid grains as compared to the fluid, which can move relatively easily. Consequently, the main part of the debris body loses some fluid so that it becomes dominated by solids. However, the tail is dominated by fluid. Since the central part of the flowing mass is dominated by solids, it increases resistance to fluid motion in two ways. First, due to the positive slope of the trailing edge of the initial mass, some fluid moves easily to the rear of the flow. Second, due to the induced higher solid volume fraction in the central part of the debris, the drag is increased. Hence, some fluid movement through the mass of debris is hindered.

[50] Another important aspect of the two-phase debris-flow simulation is the time evolution of the fluid volume

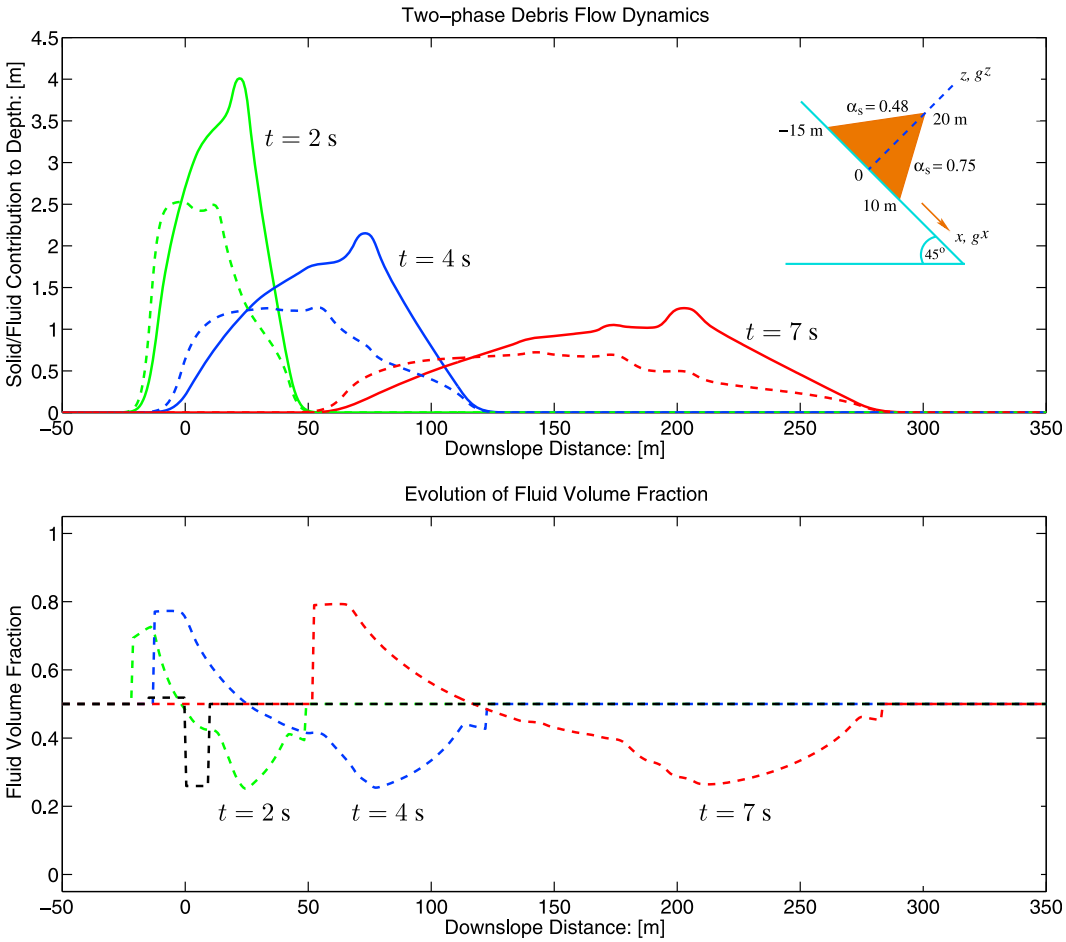

Figure 3. The upper and lower triangles are initially filled with uniform mixtures with 48% solid (UT) and 75% solid (LT), respectively, as shown in the inset (for $t = 0$) and also indicated by the step function. (top) The spatial and temporal evolution of the solid and fluid phases, represented by the solid and dashed lines, respectively. It is observed that both the front and central body of the flow are dominated by solids. Both the solid and fluid phases are continuously elongated in time by changing their shapes. The relative difference between the solid and fluid fractions that contribute to flow depth decreases in time, indicating more and more mixing as debris moves downslope. (bottom) The evolution of the fluid volume fraction, α_f, during the debris flow. Right after the mass collapse, the jump in the initial profile of α_f is immediately transformed into a strong non-linearity.

fraction (Figure 2, bottom). Initially the solid and fluid volume fractions are 0.5. Following debris collapse, there evolves a strong, non-linear dynamics of the fluid volume fraction (α_f), and at all the times the front and tail are dominated by the fluid. As the debris mass collapses and moves downslope, α_f increases in the leading and trailing edges whereas it attains minimum value somewhere in the central part of the debris mass. This behavior is also reflected by the evolution of the solid and fluid phases in Figure 2 (top).

[51] In a second simulation, the initial mass is divided into uniform mixtures of 48% solids (upper triangle) and 75% solids (lower triangle) (Figure 3). In this simulation, both the front and central body of the flow are dominated by solids. This behavior results because the fluid can not easily escape from or pass through the more densely packed solids in the front. As with the simulation of a fully uniform initial distribution of solids (Figure 2), the tail remains dominated by fluid. This is a commonly observed phenomena in granular-rich debris flows, in which the front is solids-rich, and the main body is followed by a fluid-rich tail [*Iverson*, 1997; *Iverson and Denlinger*, 2001; *Pudasaini et al.*, 2005]. Both the solid and fluid phases are continuously elongated in time. However, the relative difference between the solid and fluid fractions that contribute to flow depth decrease in time, indicating more mixing as a flow proceeds downslope. Furthermore, Figure 3 (bottom) explains the intrinsic dynamics of the debris mixture in terms of the fluid volume fraction. It is important to note that, right after the mass collapse, the jump in the initial fluid volume fraction is immediately transformed into a strong non-linearity. The fluid volume fraction decreases from the front to the middle portion of the flow, becomes minimum somewhere in the middle-right, and then increases non-linearly in the tail side of the flow.

[52] In a third simulation, the initial mass is divided into a more fluid-rich mass leading a more solids-rich mass. In this simulation, the mass is partitioned into uniform mixtures of 68% solids (upper triangle) and 32% solids (lower triangle)

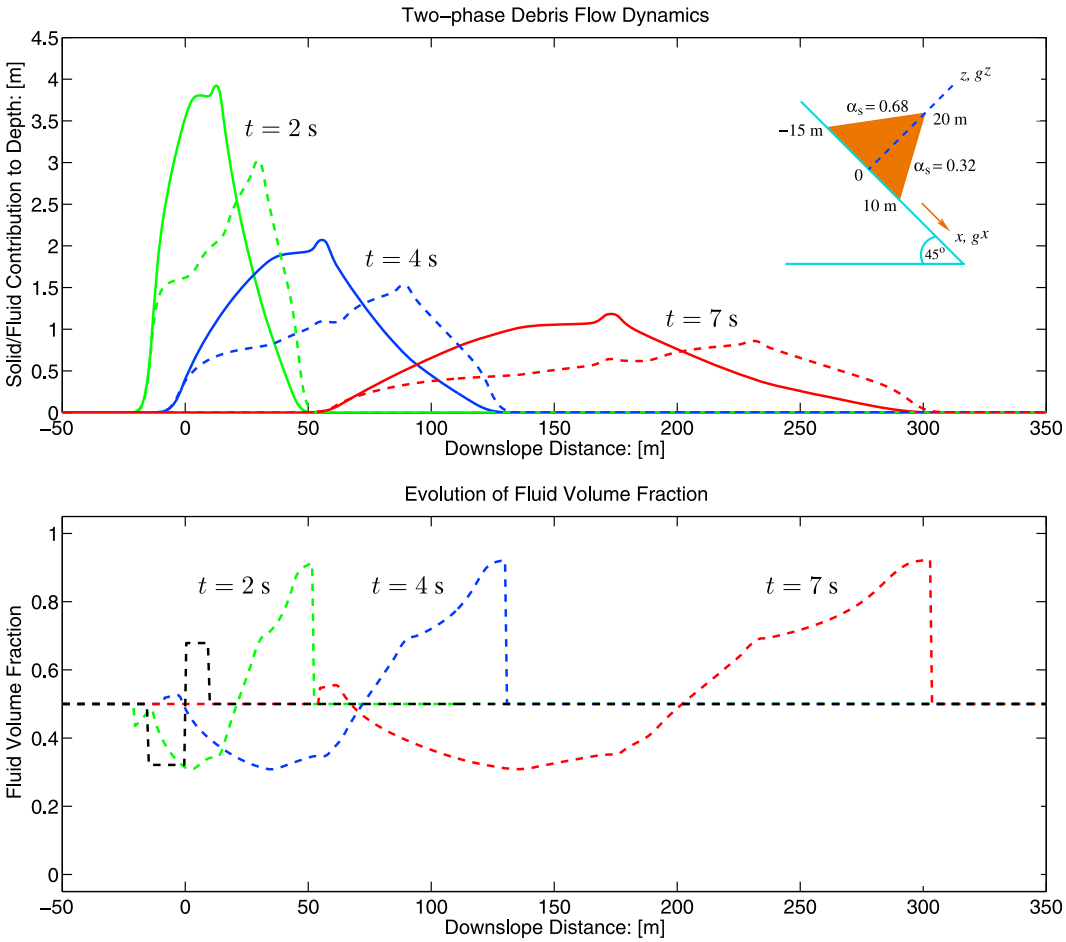

Figure 4. The upper and lower triangles are initially filled with uniform mixture with 68% solid (UT) and 32% solid (LT), respectively, as shown in the inset (for $t = 0$) and also indicated by the step function. (top) The spatial and temporal evolution of the solid and fluid phases, represented by the solid and dashed lines, respectively. The flow front and much of the central body is dominated by fluid behavior. The relative difference between the solid and fluid contributions is decreasing in time. The debris mass continuously elongates and its shape changes in time, characterizing the gradual mixing between the phases in the central part of the flowing debris and phase separation in the front and tail. (bottom) The complex non-linear dynamics of the debris mixture in terms of evolving fluid volume fraction, α_f.

(Figure 4). In this simulation, the dynamics between the solid and fluid evolution is the opposite of that shown in the prior simulation (Figure 3). From the beginning, the flow front and much of the central body is dominated by fluid behavior. Since the initial amount of fluid in the lower triangle is much greater than the volume of solids, such behavior is explained because the solid grains are dispersed and the mixture is diluted, and thus fluid easily flows downslope. In contrast, the rear of the mass is initially dominated by solids. Whereas the fluid in the front of the mass moves easily downslope, the fluid in the rear of the mass passes slowly through the solid matrix. The debris mass continuously elongates and its shape changes in time, characterizing the gradual mixing between the phases in the central part of the flowing debris and phase separation in the front and tail. As before, Figure 4 (bottom) explains the complex non-linear dynamics of the debris mixture in terms of the fluid volume fraction, α_f. However, the dynamical behavior of α_f here is quite different than in Figures 2 and 3. In the present simulation, α_f is maximum in the front of the flow, it attains the minimum value somewhere in the back side of the central body, and then increases in the tail.

[53] Fluid related longer travel distance discussed above is also observed in other debris flow simulations [*Pitman and Le*, 2005; *Pudasaini et al.*, 2005]. This reflects the higher strength of the debris material with higher amount of solid and other induced dynamical effects, such as the drag and friction. If the fluid volume fraction of the initial mass is much higher (particularly in the lower part, as in a fully saturated lower part of a mountain flank as compared to a partially saturated upper part of the same mountain flank) than the solids volume, then debris evolution shows that almost half of the frontal part is dominated by the fluid while the back side is dominated by the solid. In all simulations, the solid front and tail are tapered, whereas the fluid front and tail are parabolic, which is typical of granular and viscous deformation [*Pudasaini et al.*, 2005; *Pudasaini and Hutter*, 2007]. Therefore, there is a strong influence of the initial volume fractions leading to different deformation and different flow-margin geometries.

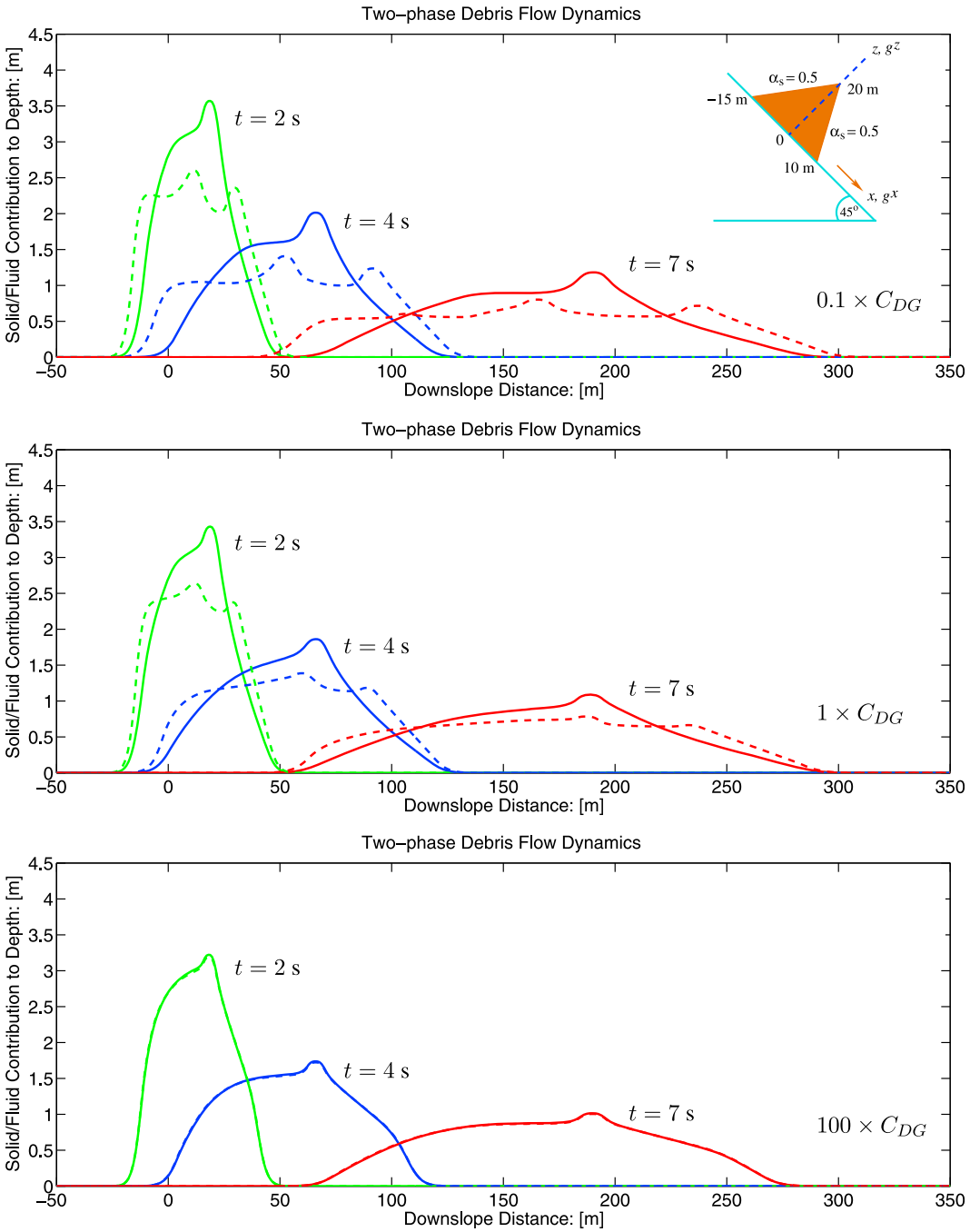

Figure 5. The generalized drag strongly influences the flow dynamics of the solid and fluid phases (represented by the solid and the dashed lines, respectively) and the entire body as a whole in two-phase debris flow. The inset shows the initial mass at $t = 0$. (middle) Drag factor 1 (normal drag), (top, bottom) have drag factors 0.1 and 100, respectively. For the drag factor 10, the simulation curves for solid and fluid are very close to each other (not shown here). Higher drag intensity (running from top to bottom) produces less relative motion (and separation between the phases), slows down the motion, and hinders the front.

7.2. Generalized Drag

[54] Drag is one of the most basic and important aspects of two-phase debris-flow, because it influences the relative motion between the solid and fluid phases. Increasing the value of the drag coefficient C_{DG} produces less relative motion (and separation) between the phases, slows down the motion, and hinders the front, because the flow front with higher drag intensity is behind the front with less drag intensity (Figure 5). Therefore, proper modeling of drag is required in order to adequately simulate two-phase debris flows.

7.3. Buoyancy

[55] Buoyancy is an important aspect of two-phase debris flow, because it enhances flow mobility by reducing the

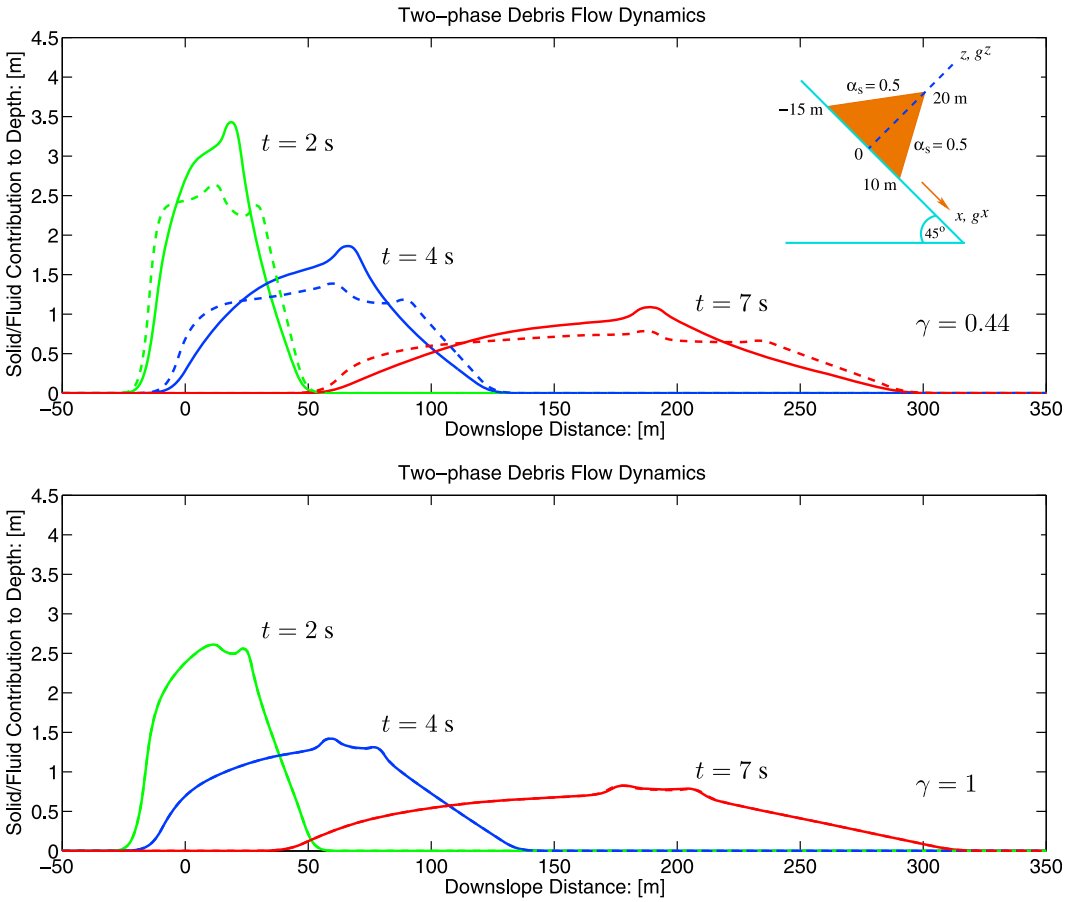

Figure 6. The buoyancy enhances the flow mobility. (top) Density ratio γ = 1,100/2,500 (normally buoyant) and (bottom) density ratio γ = 1,100/1,100 (neutrally buoyant) flow. The inset shows the initial mass at $t = 0$. Solid and fluid phases are represented by the solid and the dashed lines, respectively. As compared with the normally buoyant flow, the neutrally buoyant flow shows completely different behavior. For the latter case, the solid and fluid move together, the debris bulk mass is fluidized, the front moves substantially farther, the tail lags behind, the flow is smoother, and the overall flow height is also reduced.

frictional resistance in the mixture. Buoyancy is present as long as there is fluid in the mixture. It reduces the solid normal stress, solid lateral normal stresses, and the basal shear stress (thus, frictional resistance) by a factor $(1 - \gamma)$. The effect is substantial when the density ratio (γ) is large (e.g., in the natural debris flow). If the flow is neutrally buoyant, i.e., $\gamma = 1$, [e.g., *Bagnold*, 1954] the debris mass is fluidized and moves longer travel distances (Figure 6). Compared to a buoyant flow (Figure 6, top) the neutrally buoyant flow (Figure 6, bottom) shows completely different behavior. For the latter case, the solid and fluid phases move together, the debris bulk mass is fluidized, the front moves substantially farther, the tail lags behind, and the overall flow height is also reduced.

7.4. Virtual Mass

[56] Whereas drag force includes the phase-interaction in a uniform flow field, if the solid particles also accelerate relative to the fluid, part of the ambient fluid is accelerated, which induces a virtual mass force (thus, the solid particle induced kinetic energy of the fluid phase). Due to the virtual mass force, for present flow configuration, solid particles bring along more fluid mass with them and the fluid is pumped to the front. By focusing on the flow front, one observes that fluid flow is followed by the main debris surge (Figure 7). The solid mass loses some inertia, so it is pushed back by the fluid. The front led by a fluid flood ('muddy water') is an observable phenomena in some natural debris flows [*McArdell et al.*, 2007]. Previous debris flow models did not include the virtual mass effect.

7.5. Newtonian Viscous Stress

[57] Fluid viscosity, which can vary depending on flow composition, can substantially affect flow dynamics. To investigate this, initial upper and lower triangles of the static mass are uniformly filled with the debris consisting of 48% solids (upper triangle), and 75% solids (lower triangle), respectively. An inviscid fluid flow is characterized by $\eta_f \approx 0$, or equivalently $N_R \to \infty$ in our case for the fluid-phase. A typical viscous fluid in debris-flow can be represented by N_R = 150, 000 [see *Pudasaini et al.*, 2005]. For the present flow configuration, a typical choice of parameters g = 9.81 ms^{-2}, L = 350 m, H = 2 m, ρ_f = 1, 100 kgm^{-3}, and α_f = 0.5 suggests that the fluid-phase viscosity (η_f) is about

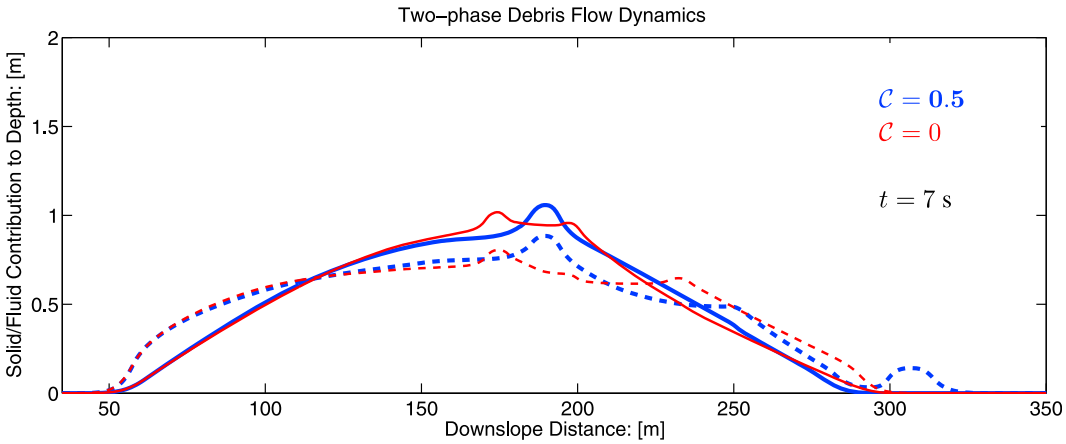

Figure 7. The virtual mass force ($\mathcal{C}$) can substantially change the dynamics of two-phase debris flow. Solid and fluid phases are represented by the solid and the dashed lines, respectively. The thin red lines ($\mathcal{C} = 0$) are without the virtual mass and the thick blue lines ($\mathcal{C} = 0.5$) are with the virtual mass ($t = 7$ s). Other simulation parameters are as in Figure 2. With the virtual mass force, the solid particles bring more fluid mass with them, fluid is pumped to the front, the front is led by fluid flood followed by the main debris surge. The solid mass loses some inertia, so it is pushed back.

2 Pas. Comparing a flow with inviscid fluid to one with viscous fluid shows that viscous stress controls the propagation of the flow front and determines how the debris mass elongates and deforms (Figure 8). The amount of fluid in the tail of a flow is substantially higher without a viscous stress compared to a flow experiencing viscous stress. Even with a small amount of fluid in the mixture, the viscous stress effect is important as it substantially reduces the deformation. Therefore, the effect of viscous resistance should be taken into account in debris flow simulation. Previous models do not systematically include the effect of viscous stress (or fluid viscosity) in two-phase debris flow dynamics.

7.6. Enhanced Non-Newtonian Viscous Stress

[58] The enhanced non-Newtonian viscous contribution to shear stress can play a significant role in appropriately controlling the two-phase debris flow dynamics. For the present configuration (in the central and the frontal part of the debris flow), $(u_f - u_s) > 0$ and $\partial\alpha_s/\partial x > 0$ (the way the solid volume fraction gradient evolves) (see Figure 2), and thus the viscous stress is down-played. Between Figures 9 (top) and 9 (bottom), there are large differences, mainly in fluid deformation, which is enhanced substantially. Figure 9 (bottom) shows that, right after the debris collapse, a large amount of fluid is pumped to the front from the middle part of the debris, and that the central part is largely dried-out. Such typical behavior may be observed in dilute debris flows where the front is largely dominated by the fluid and the tail also exhibits dominant fluid mass. Such an important physical mechanism is not yet included in classical debris flow model. Furthermore, Figures 8 and 9 reveal that the total viscous effect can substantially alter the deformation process in two-phase debris flows.

[59] Simulation results obtained for one-dimensional inclined channel flows demonstrate the differences between previously proposed Coulomb mixture and two-fluid models [*Iverson and Denlinger*, 2001; *Pudasaini et al.*, 2005; *Pitman and Le*, 2005; *Pelanti et al.*, 2008], and a new general, two-phase debris-flow model (41)–(42). The differences; as discussed in section 6, Appendices A–D, and displayed in above figures and associated texts; are substantial and are highlighted with respect to important physical aspects included in the new model, namely, the generalized drag, buoyancy, virtual mass, classical viscous stress and enhanced non-Newtonian viscous stress. Also investigated were the effects of the initial distribution of the solid volume fraction on the evolution of solid and fluid constituents, and the evolution of the fluid volume fraction.

8. Summary

[60] In this paper, a new, general two-phase debris-flow model was developed, which includes many essential physical phenomena observable in debris flows. Mohr-Coulomb plasticity is used to close the solid stress. The fluid stress is modeled as a non-Newtonian viscous stress that is enhanced (or downplayed) by the solid-volume-fraction gradient. The model includes virtual mass induced by relative accelerations between the solid and fluid phases. A generalized interfacial momentum transfer includes viscous drag, buoyancy and virtual mass forces. The *Richardson and Zaki* [1954] terminal velocity of a solid particle and a Kozeny-Carman expression for fluid flow through densely packed grains are combined to develop a new generalized drag force that covers both solid-like and fluid-like drag contributions, and allows linear and quadratic drag contributions to flow resistance. This drag force is expressed explicitly in terms of the volume fractions and densities of the solid and fluid, the terminal velocity of solid particles, particle diameter, fluid viscosity, and the particle Reynolds number. There are strong couplings between solid and fluid momentum transfer both through the interfacial momentum transfer and the solid-concentration-gradient-enhanced viscous fluid stresses. The model includes both advection and diffusion of the

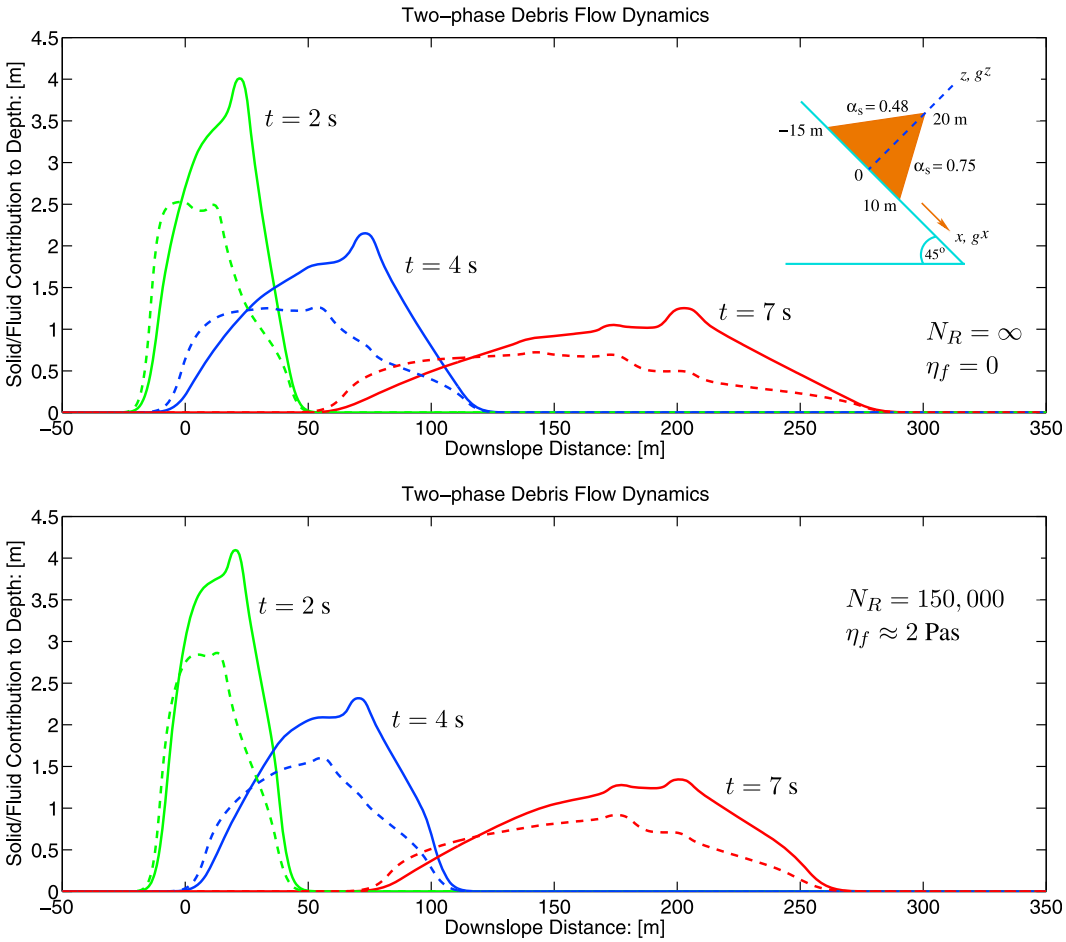

Figure 8. Initially the upper and lower triangles are uniformly filled with the debris material consisting of the solid components 48% in UT, and 75% in LT, respectively, as shown in the inset for $t = 0$. In total, the amount of fluid in the mixture is small, and that in the lower triangle, it is very small. Solid and fluid phases are represented by the solid and the dashed lines, respectively. (top) Without Newtonian viscous stress ($N_R \rightarrow \infty$, $\eta_f \approx 0$). (bottom) With Newtonian viscous stress ($N_R = 150, 000$, $\eta_f \approx 2$ Pas). The front and the rear positions, the elongation of the debris body and their deformations are different in top and bottom. This figure (bottom) (realistic) shows that the classical Newtonian viscous stress can be essential in appropriately controlling the deformation and propagation of the two-phase viscous debris flow. The amount of the fluid in the tail is substantially higher without the viscous stress (top) as compared to the same with the viscous stress (bottom). Even for the small amount of fluid in the mixture, the viscous stress effect is important as it substantially reduces the deformation.

solid-volume fraction. The proposed model unifies existing avalanche and debris flow theories including the single-phase avalanche model of *Savage and Hutter* [1989], the debris-mixture model of *Iverson and Denlinger* [2001] and *Pudasaini et al.* [2005], and the two-fluid debris-flow model of *Pitman and Le* [2005].

[61] Simulation results are presented for two-phase debris flows down an inclined channel. They demonstrate the importance of properly modeling the parameters and physical aspects of new, two-phase debris-flow model. The magnitude of the generalized drag force determines whether the flow phases remain mixed or separated, and whether the flow contracts or expands. Buoyancy enhances flow mobility. The virtual mass force alters flow dynamics by increasing the kinetic energy of the fluid. Newtonian viscous stress substantially reduces flow deformation, whereas non-Newtonian viscous stress may move a large amount of fluid from the middle part of a debris flow toward the flow front. The initial volume fraction distribution of solids strongly influences overall flow dynamics. Gradual mixing during the debris flow is observed. Strong non-linear dynamics of the fluid volume fraction demonstrates typical dynamics of the two-phase debris flow as there is a strong coupling between the solid and fluid phases. These findings are consistent with observable phenomena in natural debris flows. The simulation results indicate the potential applicability of the full model equations to adequately describe the complex dynamics of debris flows, avalanches, particle-laden, and dispersive flows. Finally, proper modeling of two-phase debris-flow dynamics should include the five dominant

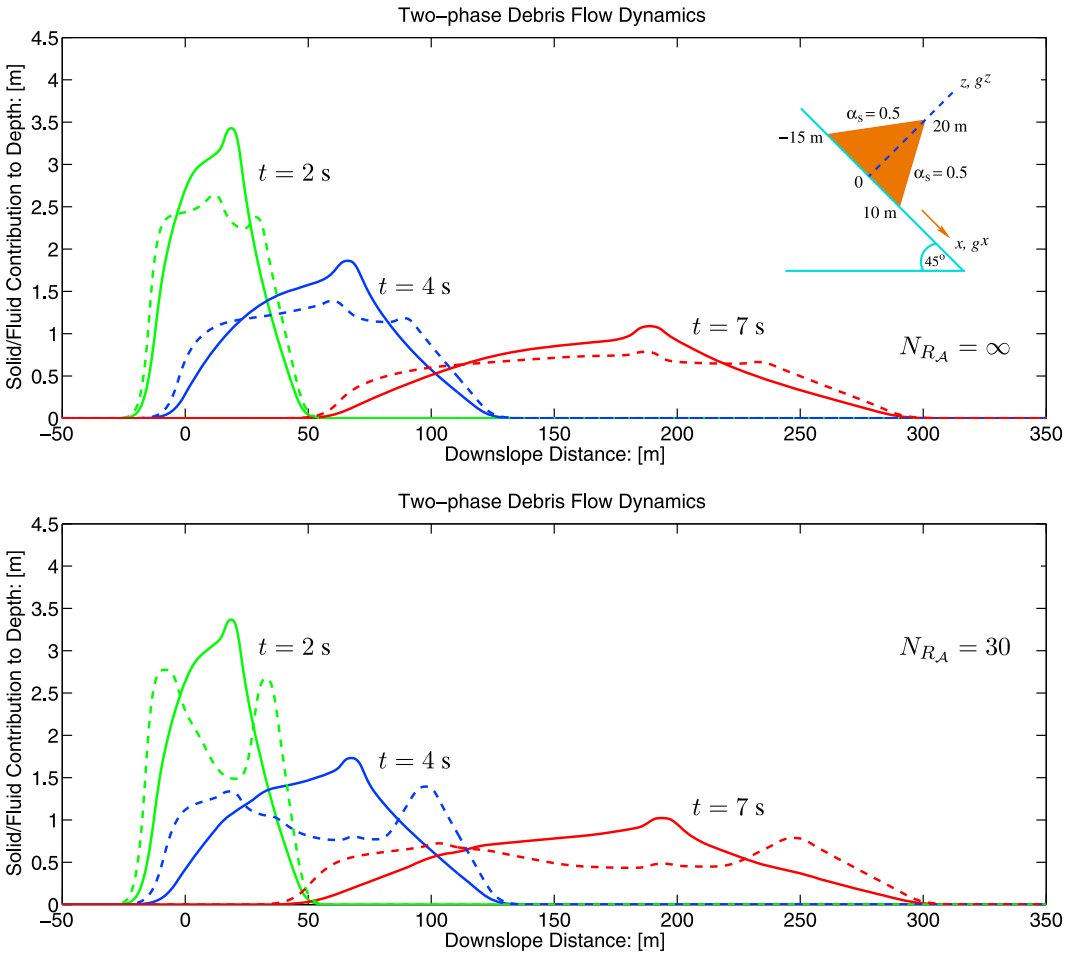

Figure 9. Solid volume fraction gradient enhanced non-classical non-Newtonian viscous stress can substantially change the dynamics of the two-phase viscous debris flows. Solid and fluid phases are represented by the solid and the dashed lines, respectively. The inset shows the initial mass at $t = 0$. (top) Without the enhanced viscous stress ($N_{R_A} \to \infty$). (bottom) With the enhanced non-Newtonian viscous stress ($N_{R_A} = 30$). This figure (bottom) shows that, right after the debris collapse, a large amount of fluid is pumped to the front from the middle part of the debris, and that the central part is largely dried-out. This is so, because for the present flow configuration, the viscous stress is downplayed in the central and frontal part of the debris body.

physical mechanisms presented and discussed in this paper, namely, drag, buoyancy, virtual mass, Newtonian viscous stress and enhanced non-Newtonian viscous stress. These mechanisms can substantially control and change the debris flow dynamics.

Appendix A: Functionality of Generalized Drag

[62] Drag increases with increasing values of the solid volume fraction (α_s) and the parameter $\mathcal{P}$, combining the solid- and fluid-like drags. Figure A1 shows the typical behavior of generalized drag coefficient $(B_d/\alpha_s)C_{DG}$ as a function of the solid volume fraction (α_s), where $B_d = \frac{4}{3}\pi r^3$ and $r = d/2$. Figure A1 (left) is for α_s in the domain [0.0, 0.75] and the Figure A1 (right) is its zoom-in in the narrow domain [0.0, 0.4], respectively. The value, $\mathcal{P} = 0.0$ corresponds to the drag coefficient of *Pitman and Le* [2005] which varies weakly with α_s. For $\mathcal{P} = 0.0$, the drag coefficient is almost 0.02 even for vanishing α_s, and the value of the drag coefficient increases very slowly as α_s increases. Even when $\alpha_s = 0.6$, the drag coefficient is below 0.2. Value of $\mathcal{P}$ between 0.0 and 1.0 combines the fluid-like and solid-like flows in the mixture. Interestingly, for values of $\mathcal{P}$ greater than zero, the generalized drag takes minimum values close to zero (for α_s close to zero) and the drag coefficient increases steadily with increasing values of α_s. Larger values of $\mathcal{P}$ correspond to more fluid flow through the solid and thus induces more drag in the flow. This means that large values of $\mathcal{P}$ corresponds to more solid in the flow. However, note that for $\mathcal{P} = 1$, which corresponds to the drag used [e.g., *Pailha and Pouliquen*, 2009] for the fluid flow through the solid, the drag coefficient becomes exceptionally large. The physically meaningful value of $\mathcal{P}$ should emerge as constrained by some experimental or field investigation and comparison between the simulation of the model equation and the experimental or the field data. From simulation

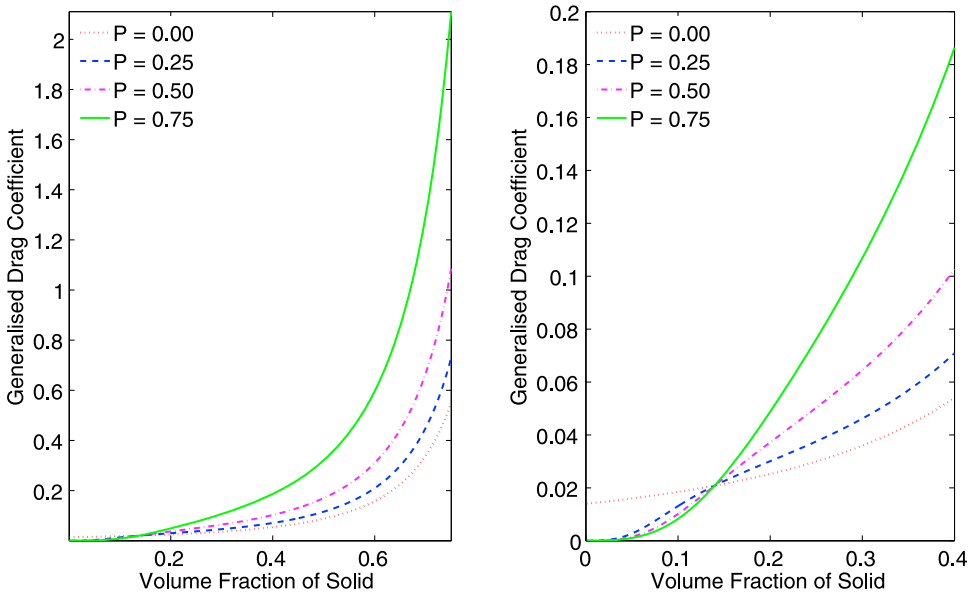

Figure A1. Generalized drag coefficient as a function of the solid volume fraction, α_s, see (9). (left) For α_s in the domain [0.0, 0.75]; (right) zoom-in in the narrow domain of α_s in [0.0, 0.4]. The parameters chosen are: $\jmath = 1, \mathcal{U}_T = 1.5\,\mathrm{ms}^{-1}$, $\rho_s = 2700\,\mathrm{kgm}^{-3}$, $\rho_f = 1200\,\mathrm{kgm}^{-3}$, $d = 1/50$ m, $g = 9.81\,\mathrm{ms}^{-2}$, and $Re_p = 1$. Drag increases with increasing values of α_s and $\mathcal{P}$, first slowly, then rapidly.

point of view, a single free parameter $\mathcal{P}$ can be utilized to model any required value of drag and fit the simulation with experiments. Further advantage of the generalized drag coefficient (9) is that different $\mathcal{P}$ values can be used to appropriately define the drags in different parts (flow regimes) of the same flowing body. It is observed in the debris flows and other particle-laden flows that some part of the body may behave as solid or granular-rich (e.g., the debris front) and some part of the body is fluid-rich (e.g., the debris tail) [see, e.g., *Iverson*, 1997; *Pudasaini et al.*, 2005; *Takahashi*, 2007]. Therefore, the new model may serve as a flexible and suitable drag model for complex, two-phase mass flows. A natural and possible choice to construct $\mathcal{P}$ is by defining it as an increasing function of α_s. Moreover, it is interesting to observe that all graphs intersect at about $\alpha_s = 0.15$ with the drag being 0.02, a typical value used in the dynamic simulation of mass flows [*Zwinger et al.*, 2003].

Appendix B: Sign Convention and Solid Stresses

[63] With the definition of the total Cauchy stress for the solid constituent (negative in compression), i.e., $\mathbf{T}_s = -p\mathbf{I} + \boldsymbol{\tau}_s$, where $\boldsymbol{\tau}_s$ is the solid extra stress tensor, the solid stress terms $-\alpha_s \nabla p + \nabla \cdot \alpha_s \boldsymbol{\tau}_s$ in *Drew* [1983] reduce to $p\nabla\alpha_s + \nabla \cdot \alpha_s \mathbf{T}_s$. Similarly, the fluid stress terms $-\alpha_f \nabla p + \nabla \cdot \alpha_f \boldsymbol{\tau}_f$ in Drew reduce to $p\nabla\alpha_f + \nabla \cdot \alpha_f \mathbf{T}_f$. Summing up the solid and fluid stress terms, one obtains $(p\nabla\alpha_s + \nabla\cdot\alpha_s\mathbf{T}_s) + (p\nabla_f + \nabla\cdot\alpha_f\mathbf{T}_f) = \nabla\cdot(\alpha_s\mathbf{T}_s + \alpha_f\mathbf{T}_f) + p\nabla(1) = \nabla\cdot(\alpha_s\mathbf{T}_s + \alpha_f\mathbf{T}_f)$, which is the (divergence of the) sum of the total solid and the fluid Cauchy stresses. However, here following *Savage and Hutter* [1989] and *Gray et al.* [1999] for convenience, the negative Cauchy stress tensor for the solid is used, i.e., $-\mathbf{T}_s$ (thus, compressive stresses are positive). With $\mathbf{T}_s = p\mathbf{I} + \boldsymbol{\tau}_s$ (which indicates compressive stresses are positive in $\boldsymbol{\tau}_s$), the solid stress terms $(p\nabla\alpha_s + \nabla\cdot\alpha_s\mathbf{T}_s)$ in *Drew* [1983] become $p\nabla\alpha_s - \nabla\cdot\alpha_s\mathbf{T}_s$, as seen in (2a).

[64] Solid stress $\mathbf{T}_s$ can be handled in different ways, including the following. Note that here $\mathbf{T}_s$ is the Cauchy stress tensor. In previous sections, following classical notations in avalanche dynamics [*Savage and Hutter*, 1989; *Gray et al.*, 1999; *Pudasaini and Hutter*, 2003], for convenience, negative Cauchy stress tensor for solid, i.e., $-\mathbf{T}_s$ is used (so for the solid the compressive stresses are positive). (*i*) One way is not to split $\mathbf{T}_s$ into pressure and the deviatoric part but treat it as a rate-independent Mohr-Coulomb plastic material. So, following *Drew* [1983] and others [*Savage and Hutter*, 1989; *Iverson and Denlinger*, 2001; *Pudasaini and Hutter*, 2003, 2007; *Pitman and Le*, 2005; *Pudasaini et al.*, 2005], do not distinguish between pressure and the extra stress but deal with $\nabla\cdot\alpha_s\mathbf{T}_s$. (*ii*) Splitting the total stress into the pressure and the extra stress, $\mathbf{T}_s = -p\mathbf{I} + \boldsymbol{\tau}_s$. Usually, in a particle laden flow, if solid phase does not behave as a viscous material, the situation can be simplified by setting $\boldsymbol{\tau}_s = 0$ (only pressure is important). In this situation, $p = p_f + p_c$, where p_f is the fluid stress, p_c is the pressure in the particles due to contacts. For relatively low concentration of solid (below the packing concentration of solid particles), $p_c = 0$. Therefore, the effective stress is simply the fluid stress, $p = p_f$ [*Drew*, 1983]. (*iii*) If the particulate phase also behaves as a viscous material, then $\mathbf{T}_s = -p\mathbf{I} + \boldsymbol{\tau}_s$, $\boldsymbol{\tau}_s \neq 0$, $\boldsymbol{\tau}_s = 2\eta_s\mathbf{D}_s$, where $\mathbf{D}_s = \frac{1}{2}\left[\nabla\mathbf{u}_s + (\nabla\mathbf{u}_s)^t\right]$ is the rate of deformation tensor for solid and η_s is the associated viscosity. This corresponds to *Ishii* [1975] with $\mathcal{A} = 0$ in $\boldsymbol{\tau}_f$ (see, (13)). However, a big concern here is how to model η_s. This could be done by using the *Jop et al.* [2006] model with $\eta_s = \eta_s(|\mathbf{D}_s|, p)/|\mathbf{D}_s|$ which is pressure- and rate-dependent.

While developing a depth-averaged model, Jop et al. rheology is difficult to handle, because the shear viscosity is highly non-linear. This could be replaced by $\boldsymbol{\tau}_s = \mu_s p\mathbf{I} + \mathcal{K}_s\eta_f\mathbf{D}_s$, where $\mu_s = \tan\delta$; $\mathcal{K}_s$ is a constant [*Pailha and Pouliquen*, 2009]. This is a pressure and rate-dependent equation, but linearly. So, for developing a depth-averaged model, if the solid phase behaves as a viscous (or visco-plastic) material then either this or similar model can be used [*Domnik and Pudasaini*, 2012]. For each of stress descriptions (*i*), (*ii*) and (*iii*), or other, one can develop different flow models. This, however, depends on the flow situations and the interest in developing a particular type of model.

Appendix C: Reduction to Previous Models

[65] As special cases of the new general debris flow model presented here, one can recover other relatively simple models available in the literature for debris flows and avalanches.

C1. Two-Fluid Model of *Pitman and Le* [2005]

[66] When both types of viscous terms (N_R and N_{R_A}) are neglected, diffusion of the solid volume fraction is not considered explicitly, virtual mass force is not present ($\mathcal{C} = 0$), the flow of fluid through solid-like or grain-rich debris flows is neglected ($\mathcal{P} = 0$), and only the linear drag force is utilized, (41)–(47) reduce to equations similar to *Pitman and Le* [2005] model. The reduced model equations are written here in conservative form and read:

$$\frac{\partial}{\partial t}[\alpha_s h u_s] + \frac{\partial}{\partial x}\left[\alpha_s h\left(u_s^2 + \beta_x\frac{h}{2}\right)\right] + \frac{\partial}{\partial y}[\alpha_s h u_s v_s] = h\mathcal{S}_{x_s}, \quad \text{(C1a)}$$

$$\frac{\partial}{\partial t}[\alpha_s h v_s] + \frac{\partial}{\partial x}[\alpha_s h u_s v_s] + \frac{\partial}{\partial y}\left[\alpha_s h\left(v_s^2 + \beta_y\frac{h}{2}\right)\right] = h\mathcal{S}_{y_s}, \quad \text{(C1b)}$$

$$\frac{\partial}{\partial t}\left[\alpha_f h u_f\right] + \frac{\partial}{\partial x}\left[\alpha_f h u_f^2\right] + \frac{\partial}{\partial y}\left[\alpha_f h u_f v_f\right] = h\mathcal{S}_{x_f}, \quad \text{(C1c)}$$

$$\frac{\partial}{\partial t}\left[\alpha_f h v_f\right] + \frac{\partial}{\partial x}\left[\alpha_f h u_f v_f\right] + \frac{\partial}{\partial y}\left[\alpha_f h v_f^2\right] = h\mathcal{S}_{y_f}, \quad \text{(C1d)}$$

where the source terms are as follows:

$$\mathcal{S}_{x_s} = \alpha_s\left[g^x - \frac{u_s}{|\mathbf{u}_s|}\tan\delta p_{b_s} - \varepsilon p_{b_s}\frac{\partial b}{\partial x}\right] - \varepsilon\alpha_s\gamma p_{b_f}\left[\frac{\partial h}{\partial x} + \frac{\partial b}{\partial x}\right] + C_{DG}\left(u_f - u_s\right), \quad \text{(C2)}$$

$$\mathcal{S}_{y_s} = \alpha_s\left[g^y - \frac{v_s}{|\mathbf{u}_s|}\tan\delta p_{b_s} - \varepsilon p_{b_s}\frac{\partial b}{\partial y}\right] - \varepsilon\alpha_s\gamma p_{b_f}\left[\frac{\partial h}{\partial y} + \frac{\partial b}{\partial y}\right] + C_{DG}\left(v_f - v_s\right), \quad \text{(C3)}$$

$$\mathcal{S}_{x_f} = \alpha_f\left[g^x - \varepsilon\left\{\frac{1}{h}\frac{\partial}{\partial x}\left(\frac{h^2}{2}p_{b_f}\right) + p_{b_f}\frac{\partial b}{\partial x}\right\}\right] - \frac{1}{\gamma}C_{DG}\left(u_f - u_s\right), \quad \text{(C4)}$$

$$\mathcal{S}_{y_f} = \alpha_f\left[g^y - \varepsilon\left\{\frac{1}{h}\frac{\partial}{\partial y}\left(\frac{h^2}{2}p_{b_f}\right) + p_{b_f}\frac{\partial b}{\partial y}\right\}\right] - \frac{1}{\gamma}C_{DG}\left(v_f - v_s\right). \quad \text{(C5)}$$

[67] Pressures and other parameters involved in these equations are:

$$\beta_x = \varepsilon K_x p_{b_s}, \beta_y = \varepsilon K_y p_{b_s}, p_{b_f} = -g^z, p_{b_s} = (1-\gamma)p_{b_f},$$
$$C_{DG} = \frac{\alpha_s\alpha_f(1-\gamma)}{\varepsilon\mathcal{U}_T\alpha_f^{M(Re_p)-1}}, \gamma = \frac{\rho_f}{\rho_s}, Re_p = \frac{\rho_f d\ \mathcal{U}_T}{\eta_f}. \quad \text{(C6)}$$

In (C1)–(C5), solid-fluid interaction is only through the drag terms. But in the general model (41)–(47), it is through the drag (C_{DG}), the virtual mass force ($\mathcal{C}$), and the solid-volume-fraction gradient enhanced viscous terms (associated with N_{R_A}). Equations similar to (C1)–(C5) were first derived by *Pitman and Le* [2005]. The following are the main differences between these reduced equations and the equations in Pitman and Le: (*a*) These equations are in conservative form. (*b*) The exponent $(1 - M)$ is different. (*c*) The Coulomb rheology and usual scaling suggested neglection of the shear stress term T_{xy} [see, e.g., *Savage and Hutter*, 1989; *Gray et al.*, 1999; *Pudasaini and Hutter*, 2007]. (*d*) The drag appeared to be scaled by the factor $1/\varepsilon$ (sections 4 and 5). This suggests that drag can be significant and dominate other terms. However, following *Savage and Hutter* [1989], *Gray et al.* [1999], *Pitman and Le* [2005], *Pudasaini et al.* [2005], etc., terms of different orders in ε are retained to include different physical and dynamical effects such as gravity, friction, basal pressure, buoyancy, fluid pressure, etc. Depending on the flow situation, locally (or even globally) one mechanism may dominate over another. Nevertheless, if the relative phase velocity is small [*Iverson and Denlinger*, 2001; *Pudasaini et al.*, 2005; *Fernandez-Nieto et al.*, 2008], density ratio is close to unity [*Bagnold*, 1954; *Pudasaini*, 2011], and either solid or the fluid volume fraction is negligible, then drag is not the dominant mechanism (or it vanishes) for the interfacial momentum transfer. (*e*) Here, the generalized drag coefficient is developed and implemented. (*f*) Basal slope effects did not appear in fluid momentum equations in *Pitman and Le* [2005] model, which are included in the above model via $\alpha_f p_{b_f}(\partial b/\partial x)$ and $\alpha_f p_{b_f}(\partial b/\partial y)$.

[68] Further differences are also seen in: (*i*) The pressure induced due to the topographic gradients, $-\varepsilon\alpha_s p_{b_s}\partial b/\partial x$, $-\varepsilon\alpha_s p_{b_s}\partial b/\partial y$ in solid momentum equations (C2)–(C3): In *Pitman and Le* [2005], these terms are respectively multiplied by the earth pressure coefficients K_x and K_y. However, traditionally these terms are free of K_x and K_y [*Savage and Hutter*, 1989; *Gray et al.*, 1999; *Pudasaini and Hutter*, 2003, 2007; *Pudasaini et al.*, 2005]. K_x and K_y should be associated with the hydraulic pressures, β_x and β_y as in (C1a)–(C1b). This difference emerges from the fact that, here for the solid phase dynamic bottom boundary, the Coulomb sliding law is applied (balance between the negative shear traction and the product of the overburden pressure and the basal friction coefficient). This does not include earth pressure coefficient [*Pudasaini and Hutter*, 2007]. However, *Pitman and Le* [2005] applied boundary conditions separately and term-wise to each terms of three basal traction vectors. This produced two basal shear related terms (α_{xy}, in their notation) and extra multiples K_x and K_y in topographic gradients. Since typically K_x and K_y vary from 0.5 (for active deformation) to 5 (for passive deformation), inclusion of these coefficients substantially alter the flow dynamics [*Pudasaini and Hutter*, 2007; *Pudasaini and*

Kroener, 2008]. (*ii*) The shear stresses (associated with α_{xy} in *Pitman and Le* [2005]) are due to the different way of implementing the bottom boundary conditions and also due to the same scaling for all stress components. However, in granular flows, normal and shear stresses are scaled differently (shear stress is a friction coefficient multiple of the normal stress) as required by the Coulomb sliding law [*Savage and Hutter*, 1989; *Pudasaini and Hutter*, 2007]. (*iii*) The topographic gradients induced fluid component normal loads ($-\varepsilon\alpha_f p_{b_f}\partial b/\partial x$, $-\varepsilon\alpha_f p_{b_f}\partial b/\partial y$ in (C4)–(C5) do not appear in *Pitman and Le* [2005] model. This is due to the fact that the basic momentum equations in (2) are fundamentally different as compared to the same in Pitman and Le. The appearance of these terms in the present model is intuitively clear, and structurally and dynamically important as analogous terms ($-\varepsilon\alpha_s p_{b_s}\partial b/\partial x$, $-\varepsilon\alpha_s p_{b_s}\partial b/\partial y$) appear in the solid source terms, the third terms in the right hand side of (C2)–(C3).

[69] I began to derive the new model with the phase-averaged equations of *Ishii* [1975], *Ishii and Zuber* [1979], and *Drew* [1983] that are different from those in *Anderson and Jackson* [1967] and *Pitman and Le* [2005]. In Pitman and Le model, the fluid volume fraction (α_f) is present only in the drag term. Because, in their basic equations, α_f appeared to be a factor in the fluid momentum equation. In the present approach, α_f is internally (with respect to differential operators) included in all terms of the fluid momentum equations (14d). Similarly, the momentum equations for the solid (14c) also include the corresponding solid volume fraction (α_s) internally in all terms. These fundamentally different basic field equations and the modeling procedures led to different sets of final model equations. In the present derivation, all these resulted in a well structured conservative form for the mass and momentum balances. This discussion implies that the reduced equations (C1)–(C6) are substantial and important advancements to the *Pitman and Le* [2005] model.

C2. Mixture Model of *Iverson and Denlinger* [2001] and *Pudasaini et al.* [2005]

[70] Next, assume that the difference between the solid and fluid velocity is negligible. So, by setting $u_f = u_s = u$ and $v_f = v_s = v$ [*Iverson*, 1997; *Iverson and Denlinger*, 2001; *Pudasaini et al.*, 2005], the new model equations (41)–(47) reduce heavily. Addition of the solid and fluid mass balances (41b) and (41c) results in a single-phase mixture mass balance, in which the effect of the solid or fluid volume fraction disappears:

$$\frac{\partial h}{\partial t}+\frac{\partial}{\partial x}(hu)+\frac{\partial}{\partial y}(hv)=0, \tag{C7}$$

where u and v are the x- and y-velocity components of the bulk (debris mixture).

[71] Similarly, adding the solid and fluid momentum balances (C1a), (C1c) and (C1b), (C1d) results in two momentum equations for the bulk in the x and y directions, respectively:

$$\begin{aligned}\frac{\partial}{\partial t}[hu]+\frac{\partial}{\partial x}\left[hu^2+\alpha_s\beta_x\frac{h^2}{2}\right]+\frac{\partial}{\partial y}[huv]&=h\mathcal{S}_x,\\ \frac{\partial}{\partial t}[hv]+\frac{\partial}{\partial x}[huv]+\frac{\partial}{\partial y}\left[hv^2+\alpha_s\beta_y\frac{h^2}{2}\right]&=h\mathcal{S}_y.\end{aligned} \tag{C8}$$

The source, pressures and other physical parameters involved in these equations are:

$$\mathcal{S}_x=\mathcal{S}_{x_s}+\mathcal{S}_{x_f},\quad \mathcal{S}_y=\mathcal{S}_{y_s}+\mathcal{S}_{y_f}, \tag{C9}$$

$$\mathcal{S}_{x_s}=\alpha_s\left[g^x-\frac{u}{|\mathbf{u}|}\tan\delta p_{b_s}-\varepsilon p_{b_s}\frac{\partial b}{\partial x}\right]-\varepsilon\alpha_s\gamma p_{b_f}\left[\frac{\partial h}{\partial x}+\frac{\partial b}{\partial x}\right], \tag{C10}$$

$$\mathcal{S}_{y_s}=\alpha_s\left[g^y-\frac{v}{|\mathbf{u}|}\tan\delta p_{b_s}-\varepsilon p_{b_s}\frac{\partial b}{\partial y}\right]-\varepsilon\alpha_s\gamma p_{b_f}\left[\frac{\partial h}{\partial y}+\frac{\partial b}{\partial y}\right], \tag{C11}$$

$$\mathcal{S}_{x_f}=\alpha_f\left[g^x-\varepsilon\left[\frac{1}{h}\frac{\partial}{\partial x}\left(\frac{h^2}{2}p_{b_f}\right)+p_{b_f}\frac{\partial b}{\partial x}-\frac{1}{\alpha_f N_R}\cdot\left\{2\frac{\partial^2 u}{\partial x^2}+\frac{\partial^2 v}{\partial y\partial x}+\frac{\partial^2 u}{\partial y^2}-\frac{\chi u}{\varepsilon^2 h^2}\right\}\right]\right], \tag{C12}$$

$$\mathcal{S}_{y_f}=\alpha_f\left[g^y-\varepsilon\left[\frac{1}{h}\frac{\partial}{\partial y}\left(\frac{h^2}{2}p_{b_f}\right)+p_{b_f}\frac{\partial b}{\partial y}-\frac{1}{\alpha_f N_R}\cdot\left\{2\frac{\partial^2 v}{\partial y^2}+\frac{\partial^2 u}{\partial x\partial y}+\frac{\partial^2 v}{\partial x^2}-\frac{\chi v}{\varepsilon^2 h^2}\right\}\right]\right], \tag{C13}$$

$$\beta_x=\varepsilon K_x p_{b_s},\quad \beta_y=\varepsilon K_y p_{b_s},\quad p_{b_f}=-g^z,\quad p_{b_s}=(1-\gamma)p_{b_f},$$
$$\gamma=\rho_f/\rho_s, N_R=\sqrt{gL}H\rho_f/\alpha_f\eta_f. \tag{C14}$$

However, α_s is no more a field variable in these drastically reduced equations. Either α_s can be treated as a parameter [*Pudasaini et al.*, 2005] or if it is assumed to be an internal variable, an extra evolution equation is required [*Iverson and Denlinger*, 2001].

[72] The reduced equations (C7)–(C14) are important extensions of the classical mixture model of *Iverson and Denlinger* [2001] and *Pudasaini et al.* [2005] with several advancements. (*a*) Here $(1-\gamma)$ includes the buoyancy force contribution, which was not present in previous models. (*b*) These equations include different physical properties of the solid and fluid constituents in the mixture, including, the solid and fluid volume fractions α_s and α_f, viscosity of the fluid (η_f), and the density ratio between the true solid and fluid densities (γ). (*c*) Although equations (C7)–(C14) are similar in form to the model equations of *Pudasaini et al.* [2005], there are some different physical mechanisms here. The differences are clearly seen in the terms associated with β_x, β_y, p_{b_s}, N_R, etc. Perhaps, the most important contributions in the above equations as compared with the classical models are the contributions of buoyancy which is present in all the solid source terms in (C10)–(C11) other than the gravity terms. Longitudinal pressure gradients associated with β_x and β_y take the buoyancy reduced normal loads. Except for the gravity terms, the solid momentum equations are dynamically enhanced by the buoyancy reduced normal load (second and third terms) or the buoyancy induced terms (fourth and fifth terms) on the right hand side of

(C10)–(C11). These new contributions are mechanically important as they clearly enhance the flow mobility. Because, in the debris mixture, the solid load is not only accounted by its volume fraction α_s as it appears in the solid loads; Coulomb force, topographic gradients and the longitudinal pressure gradients; but the contributions of all these terms (except for the gravity load) in momentum equations must also be consistent and accompanied with buoyancy or the buoyancy reduced normal load. This is so, because, buoyancy has to play its role to reduce the normal load of the solid component in the mixture. (*d*) Another essential point to note is the definition of the term N_R, which is here defined in terms of the fluid density ρ_f, which in *Iverson and Denlinger* [2001] and *Pudasaini et al.* [2005] was defined in terms of the debris bulk density ρ. (*e*) The buoyancy induced extra terms, the second square brackets on the right hand side of (C10) and (C11) are entirely new as compared to the model of *Pudasaini et al.* [2005].

[73] There are some fundamentally different solid and fluid stress mechanisms between the reduced equations (C8)–(C14) and the classical *Iverson and Denlinger* [2001] and *Pudasaini et al.* [2005] models. (*i*) Consider the fluid related contribution. Mathematically, α_f here corresponds to Λ_f in the classical models, but with different meaning. Λ_f is the ratio between the fluid pressure and the total normal load at the bed. However, α_f in the new model is exactly the fluid volume fraction in the mixture. For simple flows α_f can be treated as a parameter [*Pudasaini et al.*, 2005]. Assuming the dominant role of the fluid volume fraction distribution in the dynamics of debris flow it is important to incorporate an evolution equation for the fluid volume fraction into the system of balance equations (C7)–(C13). Considering the mathematical analogy between α_f and Λ_f, a simple approach can be used to close α_f in connection with the momentum equations. One possibility is, following *Iverson and Denlinger* [2001] and arguing that basal fluid volume fraction advects only passively along the flow directions and that it also diffuses simultaneously in the flow depth direction, α_f is described by an advection-diffusion equation $\partial\alpha_f^b/\partial t + u\partial\alpha_f^b/\partial x + v\partial\alpha_f^b/\partial y = D\left(\partial^2\alpha_f/\partial z^2\right)_b$, where b stands for bed and D is the fluid volume fraction diffusivity in the mixture. Depending on the flow situations, a full advection-diffusion equation can be considered to close α_s or α_f. Furthermore, α_s may have the largest value (close to unity) in the head and decrease in the tail side of the flow. In contrasting situation, however, if the amount of fluid is much higher compared to the solid, then α_s may diffuse in the downstream and the cross streamflow directions. So, one should choose an appropriate advection-diffusion equation (or any other closure) either to close α_s or α_f. (*ii*) Next, the stress reduction mechanism is discussed. In *Iverson and Denlinger* [2001] and *Pudasaini et al.* [2005] solid stress is expressed in terms of the effective stress: as the fluid stress increases the solid stress at the bed decreases as described by the factor $(1 - \Lambda_f)$ in all the solid source terms (gravity, Coulomb friction, and topographic gradients) and the longitudinal and lateral pressure gradients represented by β_x and β_y, respectively [*Pudasaini et al.*, 2005]. As the fluid pressure at the bed increases $(1 - \Lambda_f)$ decreases and that all the solid source terms and the pressure are reduced by this factor, which is mathematically analogous to α_s in reduced model (C7)–(C14), as both occur exactly in the same places in corresponding terms in both model equations. However, mechanically they are different: $(1 - \Lambda_f)$ is the normalized effective (solid) normal load, whereas, α_s is the solid volume fraction.

[74] Mechanically, there are two new contributions in (C7)–(C14): (*a*) The buoyancy reduced (solid) normal loads. These are present in the lateral pressures associated with β_x, and β_y (in (C8)), Coulomb friction (second terms on the right-hand sides of (C10)–(C11)) and the topographic gradients (third terms on the right hand side of (C10)–(C11)). (*b*) The last two terms associated with γ in (C10)–(C11) emerge due the buoyancy in the mixture. Buoyancy was not included in *Iverson and Denlinger* [2001] and *Pudasaini et al.* [2005] models. The present model reveals that even in situation when the fluid velocities could be approximated by the solid velocities, the buoyancy force is present. This is achieved by using the phase averaged model equations of *Ishii* [1975] and *Drew* [1983].

[75] The classical mixture theory approach [*Iverson*, 1997; *Iverson and Denlinger*, 2001; *Pudasaini et al.*, 2005; *Fernandez-Nieto et al.*, 2008] requires ad-hoc decomposition of the basal overburden pressure, gravity, and the friction, and the hydraulic pressure gradient into its 'solid contribution' $(1 - \Lambda_f)$ and 'fluid contribution' Λ_f, respectively. This division is the weakness of their formulation, because it is ad-hoc [*Hutter and Schneider*, 2010a, 2010b]. Indeed, it is dynamically necessary: because without this assumption the model equations could not be closed. The separation parameter Λ_f enters as a new field variable, for which a phenomenological closure must be postulated. Nevertheless, computational results performed for debris flows show strong influence of the fluid pressure via Λ_f and are well supported by experimental data [*Iverson*, 1997; *Iverson and Denlinger*, 2001; *Pudasaini et al.*, 2005]. The advantage of the present method is that the distribution of these force terms into the solid (α_s) and the fluid (α_f) parts are done fundamentally, and that solid- and fluid-phase stresses emerge independently. The volume fractions of solid and fluid are distributed consistently and automatically to all force terms and components. Furthermore, note that no solid and fluid volume fraction appear in the model equations in *Iverson and Denlinger* [2001] and *Pudasaini et al.* [2005], except at N_R, which was originated by manually multiplying viscous term by the fluid volume fraction [*Iverson*, 1997].

[76] The reduced system (C7)–(C14) recovers *Iverson and Denlinger* [2001] and *Pudasaini et al.* [2005] models under three conditions: (*a*) realizing $(1 - \Lambda_f)$ by α_s, (*b*) by setting $\gamma = 0$, and (*c*) replacing ρ_f by ρ in N_R. However, $\gamma = 0$ does not formally mean that $\rho_f = 0$ in their model; $\gamma = 0$ only indicates that the buoyancy force is neglected. The above discussion makes it clear that, the reduced equations are important extensions of *Iverson and Denlinger* [2001] and *Pudasaini et al.* [2005] models.

C3. Granular Flow and Avalanche Model

[77] Setting $\alpha_s = 1$ and $\gamma = 0$ in (C7)–(C14) (implying that fluid phase is absent), one obtains the reduced model for dry

granular flows or avalanches [*Savage and Hutter*, 1989; *Gray et al.*, 1999; *Pudasaini and Hutter*, 2003]:

$$\frac{\partial h}{\partial t}+\frac{\partial}{\partial x}(hu)+\frac{\partial}{\partial y}(hv)=0, \tag{C15}$$

$$\frac{\partial}{\partial t}[hu]+\frac{\partial}{\partial x}\left[hu^2+\beta_x\frac{h^2}{2}\right]+\frac{\partial}{\partial y}[huv]=h\mathcal{S}_x,$$
$$\frac{\partial}{\partial t}[hv]+\frac{\partial}{\partial x}[huv]+\frac{\partial}{\partial y}\left[hv^2+\beta_y\frac{h^2}{2}\right]=h\mathcal{S}_y, \tag{C16}$$

where, the source, pressures and other parameters involved in these reduced equations are:

$$\mathcal{S}_x=\left[g^x-\frac{u}{|\mathbf{u}|}\tan\delta p_{b_s}-\varepsilon p_{b_s}\frac{\partial b}{\partial x}\right],\ \mathcal{S}_y=\left[g^y-\frac{v}{|\mathbf{u}|}\tan\delta p_{b_s}-\varepsilon p_{b_s}\frac{\partial b}{\partial y}\right],$$
$$\beta_x=\varepsilon K_x p_{b_s},\ \beta_y=\varepsilon K_y p_{b_s}, p_{b_s}=-g^z. \tag{C17}$$

By setting $\alpha_f = 1$ (means no solid phase), the reduced mixture model (C7)–(C14) can also describe the flow of viscous fluid.

[78] The above discussions can be summarized as following. Equations (41)–(46) and the parameter definitions (47) show that these general two-phase debris flow model equations can reproduce, or almost degenerate to the previously often considered and one of the most successful avalanche and debris flow models: single phase avalanche models [*Savage and Hutter*, 1989; *Gray et al.*, 1999; *Pudasaini and Hutter*, 2003], quasi-two phase debris mixture models [*Iverson*, 1997; *Iverson and Denlinger*, 2001; *Pudasaini et al.*, 2005], and two-fluid debris flow model [*Pitman and Le*, 2005]. Furthermore, the present model equations include several new and important physical aspects of two-phase debris flows and other dispersive and particle-laden flows.

Appendix D: Model Structure and Eigenvalues

[79] The general two-phase debris flow model equations (41)–(42) are integrated for a simple flow configuration in which the debris material is released from a triangular dam and slides down an inclined one-dimensional channel. These equations can be written in equivalent form by introducing a vector of conservative state variables $\mathbf{W}=\left(h_s,h_f,m_s,m_f\right)^t$, where $h_s=\alpha_s h$, $h_f=\alpha_f h$ are the solid and fluid contributions to the debris flow height ($h_s+h_f=h$); and $m_s=\alpha_s h u_s$, $m_f=\alpha_f h u_f$, are the solid and fluid component momentum fluxes, respectively (also, see, *Pelanti et al.* [2008]). The solid and fluid-phase velocities, and the solid and fluid volume fractions can be expressed as $u_s=m_s/h_s$ and $u_f=m_f/h_f$; $\alpha_s=h_s/h$, $\alpha_f=h_f/h$, so, $\alpha_s/\alpha_f=h_s/h_f$. Equations (41)–(46) can then be written in a matrix form

$$\frac{\partial\mathbf{T}(\mathbf{W})}{\partial t}+\frac{\partial\mathbf{F}(\mathbf{W})}{\partial x}=\mathbf{S}(\mathbf{W}), \tag{D1}$$

where $\mathbf{T}=\mathbf{T}(\mathbf{W})$ is the vector of the virtual mass induced generalized conservative variables, $\mathbf{F}=\mathbf{F}(\mathbf{W})$ is the vector of transport fluxes, and $\mathbf{S}=\mathbf{S}(\mathbf{W})$ represents the source vector. They are equivalently given by:

$$\mathbf{T}=\begin{pmatrix}h_s\\ h_f\\ m_s-\gamma\mathcal{C}\left(m_f\frac{h_s}{h_f}-m_s\right)\\ m_f+\mathcal{C}\left(m_f\frac{h_s}{h_f}-m_s\right)\end{pmatrix},\qquad \mathbf{F}=\begin{pmatrix}m_s\\ m_f\\ \frac{m_s^2}{h_s}-\gamma\mathcal{C}\left(m_f^2\frac{h_s}{h_f^2}-\frac{m_s^2}{h_s}\right)+\frac{1}{2}\beta_s h_s\left(h_s+h_f\right)\\ \frac{m_f^2}{h_f}+\mathcal{C}\left(m_f^2\frac{h_s}{h_f^2}-\frac{m_s^2}{h_s}\right)+\frac{1}{2}\beta_f h_f\left(h_f+h_s\right)\end{pmatrix},$$
$$\mathbf{S}=\begin{pmatrix}0\\ 0\\ h_s\left[g^x-\frac{u_s}{|u_s|}\tan\delta p_{b_s}\right]-\varepsilon\gamma p_{b_f}h_s\frac{\partial h}{\partial x}+C_{DG}hm_{fs}\\ h_f\left[g^x-\varepsilon\left\{\frac{1}{2}p_{b_f}\frac{h^2}{h_f}\frac{\partial}{\partial x}\left(\frac{h_s}{h}\right)-\frac{h}{h_f N_R}\left(2\frac{\partial^2}{\partial x^2}\left(\frac{m_f}{h_f}\right)-\frac{\chi m_f}{\varepsilon^2 h_f h^2}\right)+\frac{h}{h_f N_{R_A}}\left(2\frac{\partial}{\partial x}\left(\frac{\partial}{\partial x}\left(\frac{h_s}{h}\right)m_{fs}\right)\right)-\frac{\xi h_s m_{fs}}{\varepsilon^2 N_{R_A}h_f h^2}\right\}\right]\\ -\frac{1}{\gamma}C_{DG}hm_{fs}\end{pmatrix}, \tag{D2}$$

where, h and $m_{fs}=(m_f/h_f-m_s/h_s)$ are used for the notational convenience in the source vector and $\beta_s=\varepsilon K p_{b_s}$, $\beta_f=\varepsilon p_{b_f}$. If $\mathcal{C}\to 0$, then $\mathbf{T}\to\mathbf{W}$.

[80] In principle, the eigenvalues of $\mathbf{A}=\partial\mathbf{F}/\partial\mathbf{W}$ can be obtained by applying the general procedure of solving the fourth order polynomial equation. However, it is mathematically challenging to obtain the exact roots of a fourth order polynomial equations in which the coefficients are very complicated and lengthy algebraic expressions. This is mainly due to the virtual mass coefficient $\mathcal{C}$. Another difficulty is associated with the relative velocity between the solid and the fluid phases [*Pitman and Le*, 2005; *Pelanti et al.*, 2008]. General analytical solution for the eigenvalues of $\mathbf{A}$ will be deferred to future works. However, to proceed further, in this paper, $\mathcal{C}$ is disregarded in obtaining the wave speed, but otherwise (D2) is considered including the effect of $\mathcal{C}$. Furthermore, to obtain some simple but semi-analytical representations of the solid and fluid wave speeds, two limiting cases are analyzed. (*i*) situation in which the solid velocity is much larger than the fluid velocity ($u_s \gg u_f$), and (*ii*) the situation in which the fluid velocity is much larger than the solid velocity ($u_f \gg u_s$). It is further rationalized that when the solid velocity is dominating, then the fluid deformation is negligible. This is an idealization of a dilute flow of particles in a relatively still background fluid.

This effectively means that the terms related to the fluid pressure gradient (β_f) can be disregarded. This rational is also applied for the fluid, i.e., when the fluid velocity dominates, then the solid deformation is negligible. In this situation, the term associated with the solid pressure gradient (β_s) is negligible. This is a limiting case in which the fluid passes through a relatively dense packing of solid. Then, **F** (equivalently **A**) is velocity- and pressure-wise decoupled into solid (first and third components) and fluid (second and fourth components).

[81] First, consider ($u_s \gg u_f$). So, the degenerated solid eigenstructure reads:

$$||\mathbf{A}_s - \lambda_s \mathbf{I}|| = \begin{pmatrix} -\lambda_s & 1 \\ -\frac{m_s^2}{h_s^2} + \frac{1}{2}\beta_s(2h_s + h_f) & \frac{2m_s}{h_s} - \lambda_s \end{pmatrix} = 0. \tag{D3}$$

This leads to the representative eigenvalues for the solid-phase: $\lambda_{s(1,3)} = m_s/h_s \pm \sqrt{\beta_s(h_s + 0.5h_f)}$. It is important to observe that λ_s take the form of the usual eigenvalues of single-phase granular flows for which $h_f = 0$ [*Pudasaini and Hutter*, 2007]. Therefore, here the solid-phase wave-celerity, $\sqrt{\beta_s(h_s + 0.5h_f)}$, is enhanced by one-half of the fluid (contribution to the debris) height ($h_f/2$) as compared to the wave-celerity of the single-phase granular flow (i.e., $\sqrt{\beta_s h_s}$). Similarly, the representative eigenvalues for the fluid-phase can be obtained: $\lambda_{f(2,4)} = m_f/h_f \pm \sqrt{\beta_f(h_f + 0.5h_s)}$. Again, importantly, λ_f takes the form of the usual eigenvalues of single-phase shallow-water flows for which $h_s = 0$ [*Pudasaini and Hutter*, 2007]. So, here the fluid-phase wave-celerity, $\sqrt{\beta_f(h_f + 0.5h_s)}$, is enhanced by one-half of the solid height ($h_s/2$) as compared to the wave-celerity of the single-phase shallow-water flow (i.e., $\sqrt{\beta_f h_f}$). Therefore, $\lambda_{1,2,3,4} = \{\lambda_{s(1,3)}, \lambda_{f(2,4)}\}$, is the representative set of eigenvalues of the model equations (D1)–(D2). With this, one can proceed to the numerical integration of the model equations. As long as $\gamma \neq 1$, $\alpha_s \neq 0$, $\alpha_s \neq 1$ and $h \neq 0$, the reduced system is strictly hyperbolic, because all λ_s and λ_f are real and distinct. Although λ_s and λ_f are not complete expressions for the eigenvalues (the complete expressions should probably include the cross coupling of β_s and β_f, and the phase velocities) they contain the basic parameters and variables of the system; namely, m_s, h_s, β_s; m_f, h_f, β_f and also cross-coupling between h_s and h_f. Such explicit and analytical expressions for λ_s and λ_f are new.

[82] Finally, it is important to note that for **F** in (D2), or for the full system (41)–(42), more complete eigenstructure (even without $\mathcal{C}$) is too complicated to be determined if the equations are to be well-posed in all flow regimes. For some flow regimes, depending on the physical parameter values and the flow dynamics, e.g., relative phase velocity, the equations may generate complex eigenvalues and thus lose the hyperbolicity. Furthermore, if the associated Jacobian is degenerated, the system loses the strict-hyperbolicity. More analysis and discussions on the eigenstructure, including the lose and gain of hyperbolicity in the multilayer flows, can be found in *Audusse* [2005], *Pitman and Le* [2005], *Bouchut and Morales* [2008], *Fernandez-Nieto et al.* [2008], *Pelanti et al.* [2008], *Castro et al.* [2010], and *Castro-Diaz et al.* [2011].

Notation

A_d projected area of a particle.
$\mathcal{A}$ mobility of fluid at interface.
B_d particle volume.
b basal-surface of flow.
C_{DG} generalized drag coefficient.
C_{VM} virtual mass coefficient.
C_{VMG} generalized virtual mass coefficient.
$\mathcal{C} = C_{VM}$, virtual mass coefficient.
$\tilde{\mathcal{C}} = (\alpha_s/\alpha_f)\mathcal{C}$.
D fluid volume fraction diffusivity in debris mixture.
$\mathbf{D}_s$ rate of deformation tensor for solid.
d particle diameter.
$\mathbf{F}_D$ drag force.
F_D magnitude of $\mathbf{F}_D$.
F a scalar function.
$\mathbf{f}$ body force density.
f stands for fluid-phase.
f a scalar function.
$\mathcal{F}$ fluid-like contribution in generalized drag, C_{DG}.
$\mathcal{G}$ solid-like contribution in generalized drag, C_{DG}.
g gravity constant.
g a scalar function.
g^x, g^y, g^z components of gravitational acceleration.
H typical height of debris flow.
$h = h_s + h_f$, debris flow height.
$h_f = \alpha_f h$, fluid contribution to flow height.
$h_s = \alpha_s h$, solid contribution to flow height.
$\mathbf{I}$ identity matrix.
$\jmath$ exponent for linear or quadratic drag.
K, K_x, K_y earth pressure coefficients.
$\mathcal{K}$ hydraulic conductivity.
$\mathcal{K}_s$ a constant.
L typical extent of debris flow.
$\mathbf{M}$ interfacial force density/interfacial momentum transfer.
$\mathbf{M}_D$ force associated with viscous drag.
$\mathbf{M}_f$ interfacial momentum transfer for fluid.
$\mathbf{M}_s$ interfacial momentum transfer for solid.
$\mathbf{M}_{VM}$ force associated with virtual mass.
M a parameter depending on Reynolds number.
M_D magnitude of $\mathbf{M}_D$.
$m_f = \alpha_f h u_f$, fluid momentum flux.
$m_s = \alpha_s h u_s$, solid momentum flux.
N normal pressure.
$N_R = \sqrt{gL}\rho_f H/\alpha_f \eta_f$, quasi-Reynolds number.
$N_{R_A} = \sqrt{gL}\rho_f H/\mathcal{A}\eta_f$, quasi-Reynolds number/mobility number.
$\mathbf{n}$ unit normal vector.
$\mathcal{P}$ parameter combining solid-like and fluid-like drag contributions.
p fluid pressure.
p_{b_f}, p_{b_s} effective fluid, solid pressure at base.

Re_p = $\rho_f d\mathcal{U}_T/\eta_f$, particle Reynolds number.
r = $d/2$, particle radius.
$\mathbf{S}$ shear stress.
$\mathcal{S}$ source terms.
s stands for solid-phase.
s free-surface of flow.
$\mathbf{T}$ total stress.
$\mathbf{T}_f$ fluid stress.
$\mathbf{T}_s$ solid stress.
T solid stress components.
t time.
t transpose operator.
$\mathcal{U}_s$ particle sedimentation velocity.
$\mathcal{U}_T$ terminal velocity of a particle.
$\mathbf{u}_f$ = (u_f, v_f, w_f), fluid velocity.
$\mathbf{u}_s$ = (u_s, v_s, w_s), solid velocity.
u x velocity of bulk debris.
v y velocity of bulk debris.
$\mathbf{W}$ = $(h_s, h_f, m_s, m_f)^t$, vector of conservative variables.
x, y, z coordinate lines/flow directions.
α_f volume fraction for fluid.
α_s volume fraction for solid.
α_{ck} Kozeny-Carman packing of spheres.
β_f, β_s lateral hydraulic pressure parameters for fluid, solid.
β_x, β_y lateral hydraulic pressure parameters.
γ = ρ_f / ρ_s, density ratio.
δ internal friction angle.
ε = H/L, aspect ratio.
ζ channel slope angle.
η_s solid viscosity.
η_f fluid viscosity.
κ permeability.
Λ_f ratio between basal pore fluid pressure and total normal stress.
λ_f, λ_s eigenvalue for fluid-, solid-phase.
μ = $\tan\delta$, basal friction coefficient.
ν a parameter.
ξ vertical distribution of α_s.
ρ debris bulk density.
ρ_f fluid phase density.
ρ_s solid phase density.
$\boldsymbol{\tau}_f$ extra stress for fluid.
$\boldsymbol{\tau}_s$ extra stress for solid.
ϕ basal friction angle.
χ vertical shearing of fluid velocity.
$\bar{*}$ depth-averaged value of *.
∇ gradient operator.
$\otimes$ tensor product.

[83] **Acknowledgments.** I thank the German Science Foundation (DFG) for the financial support through grants PU 386/1-1, 2: *Transition of a Granular Flow into the Deposit.* I am grateful to Stephen A. Miller, Kolumban Hutter, Sebastian Noelle, Anthony Thornton, and Christian Kroener for fruitful discussions. I sincerely thank three anonymous referees, associate editor and the editor, Alexander Densmore, for their careful reading of the manuscript, constructive reviews and valuable suggestions that substantially helped to increase the clarity and quality of the paper.

References

Anderson, T. B., and R. Jackson (1967), A fluid mechanical description of fluidized beds: Equations of motion, *Ind. Eng. Chem. Fundam.*, *6*, 527–539.

Audusse, E. (2005), A multilayer Saint-Venant model: Derivation and numerical validation, *Discrete Cont. Dyn. Syst., Ser. B*, *5*(2), 189–214.

Bagnold, R. A. (1954), Experiments on a gravity-free dispersion of large solid spheres in a Newtonian fluid under shear, *Proc. R. Soc. Lond., Ser. A*, *225*, 49–63.

Bouchut, F., and T. Morales (2008), An entropy satisfying scheme for two-layer shallow water equations with uncoupled treatment, *ESAIM: Math. Modell. Numer. Anal.*, *42*(4), 683–698.

Carman, P. C. (1937), Fluid flow through granular beds, *Trans. Inst. Chem. Eng.*, *15*, 150–166.

Carman, P. C. (1956), *Flow of Gases Through Porous Media*, Butterworths, London.

Castro, M., J. T. Frings, S. Noelle, C. Pares, and G. Puppo (2010), On the hyperbolicity of two- and three-layer shallow water equations, *Rep. 314*, 8 pp., Inst. für Geom. und Prakt. Math., Aachen Univ., Aachen, Germany.

Castro-Diaz, M. J., E. D. Fernandez-Nieto, J. M., Gonzalez-Vida, and C. Pares-Madronal (2011), Numerical treatment of the loss of hyperbolicity of the two-layer shallow-water system, *J. Sci. Comput.*, *48*(1–3), 16–40.

Chen, C. L. (1988), Generalized viscoplastic modelling of debris flow, *J. Hydraul. Res.*, *114*(3), 237–258.

Crosta, G. B., H. Chen, and C. F. Lee (2004), Replay of the 1987 Val Pola Landslide, Italian Alps, *Geomorphology*, *60*, 127–146.

Domnik, B., and S. P. Pudasaini (2012), Full two-dimensional rapid chute flows of simple viscoplastic granular materials with a pressure-dependent dynamic slip-velocity and their numerical simulations, *J. Non-Newtonian Fluid Mech.*, *173–174*, 72–86.

Drew, D. A. (1983), Mathematical modelling of two-phase flow, *Ann. Rev. Fluid Mech.*, *15*, 261–291.

Drew, D. A., and R. T. Lahey Jr. (1987), The virtual mass and lift force on a sphere in rotating and straining inviscid flow, *Int. J. Multiphase Flow*, *13*, 113–121.

Fernandez-Nieto, E. D., F. Bouchut, D. Bresch, M. J. Castro Diaz, and A. Mangeney (2008), A new Savage-Hutter type model for submarine avalanches and generated tsunami, *J. Comput. Phys.*, *227*, 7720–7754.

Fischer, J.-T., J. Kowalski, and S. P. Pudasaini (2012), Topographic curvature effects in applied avalanche modeling, *Cold Reg. Sci. Tech.*, *74–75*, 21–30.

George, D. L., and R. M. Iverson (2011), A two-phase debris-flow model that includes coupled evolution of volume fractions, granular dilatancy, and pore-fluid pressure, *Ital. J. Eng. Geol. Environ.*, doi:10.4408/IJEGE.2011-03.B-047, in press.

Gray, J. M. N. T., M. Wieland, and K. Hutter (1999), Gravity-driven free surface flow of granular avalanches over complex basal topography, *Proc. R. Soc, A*, *455*, 1841–1874.

Hungr, O. (1995), A model for the runout analysis of rapid flow slides, debris flows, and avalanches, *Can. Geotechn. J.*, *32*, 610–623.

Hutter, K., and L. Schneider (2010a), Important aspects in the formulation of solid-fluid debris-flow models. Part I. Thermodynamic implications, *Continuum Mech. Thermodyn.*, *22*, 363–390.

Hutter, K., and L. Schneider (2010b), Important aspects in the formulation of solid-fluid debris-flow models. Part II. Constitutive modelling, *Continuum Mech. Thermodyn.*, *22*, 391–411.

Hutter, K., B. Svendsen, and D. Rickenmann (1996), Debris flow modelling: A review, *Continuum Mech, Thermodyn.*, *8*, 1–35.

Ishii, M. (1975), *Thermo-Fluid Dynamic Theory of Two-Phase Flow*, Eyrolles, Paris.

Ishii, M., and T. Hibiki (2006), *Thermo-Fluid Dynamics of Two-Phase Flow*, Springer, New York.

Ishii, M., and N. Zuber (1979), Drag coefficient and relative velocity in bubbly, droplet or particulate flows, *AIChE J.*, *25*, 843–855.

Iverson, R. M. (1997), The physics of debris flows, *Rev. Geophys.*, *35*(3), 245–296.

Iverson, R. M., and R. P. Denlinger (2001), Flow of variably fluidized granular masses across three-dimensional terrain: 1. Coulomb mixture theory, *J. Geophys. Res.*, *106*(B1), 537–552.

Jop, P., Y. Forterre, and O. Pouliquen (2006), A constitutive law for dense granular flow, *Nature*, *441*, 727–730.

Kolev, N. I. (2007), *Multiphase Flow Dynamics: Thermal and Mechanical Interactions*, 3rd ed., Springer, New York.

Kozeny, J. (1927), Ueber kapillare Leitung des Wassers im Boden, *Sitzungsber Akad. Wiss. Wien*, *136*(2), 271–306.

Kytoma, H. K. (1991), Viscous particle interactions and their effect on kinematic wave propagation, *Chem. Eng. Commun.*, *105*(1), 27–42.

Legros, F. (2002), The mobility of long-runout landslides, *Eng. Geol.*, *63*, 301–331.

Lyczkowski, R. W., D. Gidaspow, C. Solbrig, and E. D. Hughes (1978), Characteristics and stability analyses of transient one-dimensional two-phase flow equations and their finite difference approximations, *Nucl. Sci. Eng.*, *66*, 378–396.

Maxey, R. M., and J. J. Riley (1993), Equation of motion for a small sphere in a non-uniform flow, *Phys. Fluids*, *26*, 883–889.
McArdell, B. W., P. Bartelt, and J. Kowalski (2007), Field observations of basal forces and fluid pore pressure in a debris flow, *Geophys. Res. Lett.*, *34*, L07406, doi:10.1029/2006GL029183.
Nessyahu, H., and E. Tadmor (1990), Non-oscillatory central differencing for hyperbolic conservation laws, *J. Comput. Phys.*, *87*, 408–463.
O'Brien, J. S., P. J. Julien, and W. T. Fullerton (1993), Two-dimensional water flood and mudflow simulation, *J. Hyd. Eng.*, *119*(2), 244–261.
Ouriemi, M., P. Aussillous, and E. Guazzelli (2009), Sediment dynamics. Part 1: Bed-load transport by laminar shearing flows, *J. Fluid Mech.*, *636*, 295–319.
Pailha, M., and O. Pouliquen (2009), A two-phase flow description of the initiation of underwater granular avalanches, *J. Fluid Mech.*, *633*, 115–135.
Pelanti, M., F. Bouchut, and A. Mangeney (2008), A Roe-Type scheme for two-phase shallow granular flows over variable topography, *Math. Model. Numer. Anal.*, *42*, 851–885.
Pitman, E. B., and L. Le (2005), A two-fluid model for avalanche and debris flows, *Philos. Trans. R. Soc. A*, *363*, 1573–1602.
Pudasaini, S. P. (2011), Some exact solutions for debris and avalanche flows, *Phys. Fluids*, *23*(4), 043301, doi:10.1063/1.3570532.
Pudasaini, S. P., and B. Domnik (2009), Energy consideration in accelerating rapid shear granular flows, *Nonlin. Processes Geophys.*, *16*, 399–407.
Pudasaini, S. P., and K. Hutter (2003), Rapid shear flows of dry granular masses down curved and twisted channels, *J. Fluid Mech.*, *495*, 193–208.
Pudasaini, S. P., and K. Hutter (2007), *Avalanche Dynamics: Dynamics of Rapid Flows of Dense Granular Avalanches*, 602 pp., Springer, New York.
Pudasaini, S. P., and C. Kröner (2008), Shock waves in rapid flows of dense granular materials: Theoretical predictions and experimental results, *Phys. Rev. E*, *78*, 041308, doi:10.1103/PhysRevE.78.041308.
Pudasaini, S. P., Y. Wang, and K. Hutter (2005), Modelling debris flows down general channels, *Nat. Hazards Earth Syst. Sci.*, *5*, 799–819.
Pudasaini, S. P., K. Hutter, S.-S. Hsiau, S.-C. Tai, Y. Wang, and R. Katzenbach (2007), Rapid flow of dry granular materials down inclined chutes impinging on rigid walls, *Phys. Fluids*, *19*(5), 053302, doi:10.1063/1.2726885.
Richardson, J. F., and W. N. Zaki (1954), Sedimentation and fluidization: Part 1, *Trans. Inst. Chem. Eng.*, *32*, 35–53.
Rivero, M., J. Magnaudet, and J. Fabre (1991), Quelques resultants nouveaux concernat les forces exercees sur une inclusion spherique par un ecoulement accelere, *C. R. Acad. Sci., Ser. II*, *312*, 1499–1506.
Sano, O. (2011), Flow-induced waterway in a heterogeneous granular material, *Comp. Phys. Commun.*, *182*, 1870–1874.
Savage, S. B., and K. Hutter (1989), The motion of a finite mass of granular material down a rough incline, *J. Fluid Mech.*, *199*, 177–215.
Sosio, R., G. B. Crosta, and O. Hungr (2008), Complete dynamic modeling calibration for the Thurwieser rock avalanche (Italian Central Alps), *Eng. Geol.*, *100*, 11–26.
Strom, A. L., and O. Korup (2006), Extremely large rockslides and rock avalanches in the Tien Shan Mountains, Kyrgyzstan, *Landslides*, *3*, 125–136.
Tai, Y.-C., S. Noelle, J. M. N. T. Gray, and K. Hutter (2002), Shock-capturing and front-tracking methods for granular avalanches, *J. Comput. Phys.*, *175*, 269–301.
Takahashi, T. (1991), *Debris Flow*, Balkema, Rotterdam, Netherlands.
Takahashi, T. (2007), *Debris Flow: Mechanics, Prediction and Countermeasures*, Taylor and Francis, New York.
Zahibo, N., E. Pelinovsky, T. Talipova, and I. Nikolkina (2010), Savage-Hutter model for avalanche dynamics in inclined channels: Analytical solutions, *J. Geophys. Res.*, *115*, B03402, doi:10.1029/2009JB006515.
Zwinger, T., A. Kluwick, and P. Sampl (2003), Numerical simulation of dry-snow avalanche flow over natural terrain, in *Dynamic Response of Granular and Porous Materials under Large and Catastrophic Deformations*, *Lecture Notes in Appl. and Comput. Mech.*, vol. 11, edited by K. Hutter and N. Kirchner, pp. 161–194, Springer, Berlin.